
Article:
Nawaz, M, Heitor, A orcid.org/0000-0002-2346-8250 and Sivakumar, M (2022) Development and evaluation of a novel geopolymer based on basalt rock waste and ground granulated blast furnace slag. Australian Journal of Civil Engineering, 20 (2). pp. 424-443. ISSN 1448-8353

https://doi.org/10.1080/14488353.2021.1995132

Development and evaluation of a novel geopolymer based on basalt rock waste and ground granulated blast furnace slag

Mohsin Nawaz†

MSc Engg

PhD Candidate, School of Civil, Mining and Environmental Engineering, Faculty of Engineering and Information Sciences, University of Wollongong, Wollongong, NSW 2522, Australia

Assistant Professor, University of Central Punjab, Lahore, Pakistan

Ana Heitor

LicEng (Lisbon), MEng (Kyoto), PhD (Wollongong), MIAust

School of Civil Engineeing, University of Leeds, Leeds, UK

formerly Centre for Geomechanics and Railway Engineering, School of Civil, Mining and Environmental Engineering, University of Wollongong, Wollongong, NSW 2522, Australia

Muttucumaru Sivakumar

BSc Engg Hons (SLanka), MEng (AIT), PhD (Newcastle), FIEAust

Associate Professor, School of Civil, Mining and Environmental Engineering, University of Wollongong, Wollongong, NSW 2522, Australia

†Author for correspondence:
Mohsin Nawaz
School of Civil, Mining and Environmental Engineering,
Faculty of Engineering and Information Sciences,
University of Wollongong,
Wollongong, NSW
Australia
Ph: +61466056125
Email: mn291@uowmail.edu.au

To be submitted to: Australian Journal of Civil Engineering
Number of words (including abstract, references, figures etc.): 8945
Number of Tables:4
Number of Figures:18

Abstract

Increase in industrial and construction activities has led to an enormous rise in waste generation and its hazardous impacts on the environment. Quarrying of rocks and manufacturing of artificial sands for civil engineering projects leads to the dumping of rock waste dust, which is a source of landfill problems. Further, excessive energy requirements for cement manufacturing, higher greenhouse gas emissions and rapid depletion of natural resources have focused the research towards the development of environment friendly and sustainable materials such as geopolymers. In this paper, a novel geopolymer has been developed from industrial wastes such as basalt rock fines considering partial replacement with ground granulated blast furnace slag (GGBFS) up to 30%. After a detailed mix-design investigation, the optimum molarity (M) of the sodium hydroxide solution was found to be 8M whereas the optimum ratio (R) of sodium silicate to sodium hydroxide solution as 0.75. Unconfined compressive strength (UCS) evaluation showed 7-day strengths up to 34 MPa, comparable to geopolymers based on conventional precursor materials. The scanning electron microscopy (SEM) imaging of the specimens revealed a dense geopolymer gel formation resulting in a homogeneous and compact microstructure. As a result, this innovative material produced can be used as an alternative, sustainable and cost-effective construction material.

Keywords: geopolymers, basalt rock waste, blast furnace slag, unconfined strength, microstructure

1. Introduction

Basalt rocks, having a high alumina and silica content, can be a potential raw material for the manufacturing of geopolymers (Davidovits, 1989; Duxson et al., 2007; Khale and Chaudhary, 2007; Lahoti et al., 2017). Large quantities of quarry fines generated as an industrial waste are being deposited in landfills which can cause serious environmental issues (Eliche-Quesada et al., 2020). A quarry on an average produces 20,000-30,000 tons per annum of rock fines, which are mostly dumped into landfill sites, thus contributing to environmental hazards. Currently, the waste by-product associated with rock quarrying activities of basalt rocks (basalt rock fines or dust) has limited application in the agricultural industry as a soil amendment agent (Nunes et al., 2014).

Geopolymers are synthesized as a result of activation of aluminosilicate source by a highly concentrated alkali hydroxide or silicate solution (Ahmad et al., 2021; Azevedo et al., 2020; Davidovits, 1989; Mathew and Issac, 2020; Serag Faried et al., 2020; Xie et al., 2020). The aluminosilicate compound goes through the dissolution phase responsible for transformation of aluminosilicate particles (Duxson et al., 2007; Rios et al., 2019; Wong et al., 2020; Xie and Fang, 2019). High pH levels of the activator solution (generally ranging from 10 to 13), dissolve the amorphous aluminate and silicate species and result in a highly saturated aluminosilicate solution thus forming a gel-like structure. The large oligomer networks promote the formation of a bi-phasic hydrated gel. The linkages of the gel network enhance with time and the system hardens to form a three-dimensional aluminosilicate network generally known as geopolymer.

The increase in construction activities worldwide in the past few decades has resulted in an increasing demand for Ordinary Portland Cement (OPC). It has been estimated that the global production of cement in 2016 was nearly 4 billion tonnes (Andrew, 2018; Phummiphan

et al., 2018). While enhanced strength and reduced shrinkage are achieved for concrete applications using cement (e.g. better bonding of aggregates), its manufacturing process is highly energy intensive leading to excessive greenhouse gases emissions especially carbon dioxide (CO_2) (Akbar et al., 2021; Duxson et al., 2007; Hassan et al., 2020; Hoppe Filho et al., 2021; Nawaz et al., 2020; Shobeiri et al., 2021; Sontia Metekong et al., 2020; Zhang et al., 2013). For instance, approximately, one tonne of cement produces around 900 kg of $CO_{2\text{-}e}$ and consumes about 5 Gigajoules of energy (Stafford et al., 2016). The need for alternative more sustainable cementitious binders, such as geopolymers has been receiving significant attention in the past decade. The geopolymer raw materials are often by-products from industrial processes (e.g. fly ash and blast furnace slag) and their usage helps to promote sustainable construction practices both financially (cost reduction up to 30%) and environmentally (greenhouse gas emission reduction up to 80%) (Erfanimanesh and Sharbatdar, 2020; Kolovos et al., 2013; Shobeiri et al., 2021; Zhang et al., 2013).

Past studies have focused on the development of geopolymers based on various natural materials (e.g. metakaolin, kaolin, rice husk ash, and bagasse) as well as industrial wastes (e.g. fly ash, blast furnace slag) in order to supplement the requirement for environment friendly construction materials (Arulrajah et al., 2017; Chindaprasirt et al., 2007; Hardjito et al., 2005; Izquierdo et al., 2009; Malkawi et al., 2020; Palomo et al., 1999; Ramlochan et al., 2000; Samarakoon et al., 2021). For instance, geopolymers derived from metakaolin, sedimentary rock powders, fly ash, blast furnace slag and other materials have shown comparable compressive strengths (Görhan and Kürklü, 2014; Lahoti et al., 2017; Nath and Kumar, 2019; Top and Vapur, 2018) as well as enhanced the chloride and sulphate resistance characteristics to that of conventional cementitious binders (Kwasny et al., 2018; Reddy et al., 2013; Sata et al., 2012; Sturm et al., 2018; Wasim et al., 2021).

115 In this study, a novel approach to produce a sustainable geopolymer based on two
116 industrial wastes (basalt rock fines and ground granulated blast furnace slag) has been
117 proposed. The main objectives of the research were to find optimum values of the synthesis
118 parameters required in the formation of basalt fines and ground granulated blast furnace slag
119 (GGBFS) geopolymer. In the first phase of testing, several combinations of synthesis
120 parameters were used in order to prepare different mix designs of the basalt fines geopolymer.
121 In the second phase, the ground granulated blast furnace slag (GGBFS) was used to partially
122 replace the basalt rock fines by 10, 20 and 30% by mass. The optimum values of all the
123 parameters were determined in order to achieve higher compressive strength and better
124 workability characteristics. The possible application of the proposed geopolymer can result in
125 substantial economic and environmental benefits as the source materials are waste by-products
126 and their disposal currently involves stockpiling in landfills. The reprocessing and reuse of
127 these waste materials to generate a cleaner value added product will contribute to enhanced
128 sustainable construction practices, therefore making a step towards zero waste initiative.

129

130 **2. Experimental program**

131 *2.1 Raw materials*

132 The proposed geopolymer has four main materials as its components. The two precursor
133 materials used were basalt rock fines and ground granulated blast furnace slag. The basalt rock
134 fines were obtained from a quarry in the Illawarra region of New South Wales (Australia)
135 whereas ground granulated blast furnace slag (GGBFS) was provided by Australasian Slag
136 Association (ASA). Both are classified as industrial wastes and result from the manufacturing
137 processes of sands and steel, respectively. The alkaline activator solution was prepared using
138 98% pure sodium hydroxide pellets manufactured by Bondall (Australia) and D-grade sodium

139 silicate solution (specific gravity= 1.53 and SiO_2/Na_2O modulus ratio=2.0) which was supplied
140 by PQ Corporation (Australia).

141

142 *2.2 Material characterisation*

143 To investigate the general geotechnical characteristics of basalt fines, several
144 identification and characterisation tests such as particle size analysis, Atterberg limits analysis,
145 specific gravity analysis and standard Proctor compaction tests were performed. The particle
146 size analysis of the basalt fines was carried out using Mastersizer 3000 laser diffraction particle
147 size analyser (manufactured by Malvern panalytical Ltd.) having a measurement range from
148 0.01 to 3500 µm. Figure 1 shows the particle size distribution curve for the basalt fines. The
149 D_{10}, D_{30} and D_{50} are 3.5µm, 17.5µm and 40.5µm, respectively.

150 The compaction characteristics were determined using standard compaction tests in
151 accordance with AS 1289.5.1.1-2017. The maximum dry unit weight and optimum moisture
152 content obtained were 18.8 kN/m^3 and 13.5%, respectively as shown in Figure 2. The specific
153 gravity of basalt fines (AS 1289.3.5.1-2006) was found to be 2.76. The basalt fines showed a
154 liquid limit of 24.0%, plastic limit of 17.6% and a plasticity index of 6.4% (AS 1289.3.1.1-
155 2009 and AS 1289.3.2.1-2009). Thus, the basalt fines may be classified as clayey silt or CL-
156 ML (AS 1726-2017).

157 Scanning electron microscopy (SEM) technique was employed to investigate the
158 microstructure of basalt fines using JEOL JSM-6490LV scanning electron microscope. Low
159 vacuum environment was maintained in the chamber at a pressure of 40 Pa, accelerating
160 voltage of 16 kV and the spot size was kept at 63 nm during the sample analysis. The images
161 taken at different magnifications (x250, x500, x1000 and x2000) are shown in Figure 3. The
162 scanning electron micrographs revealed that the basalt fines particles are sharp-edged having

irregular and angular surfaces that would assist in greater interlocking and thus denser geopolymer gel formation. A combination of different particle sizes is expected to assist in pore size reduction of geopolymer matrix. Indeed, the voids in the sample imaged under the microscope, were around 1 to 4 µm and were likely to be reduced during the geopolymerisation process. The energy dispersive spectroscopy (EDS) analysis showed high Si and Al peaks, as highlighted in Figure 4, which was a confirmation of basalt fines being a suitable aluminosilicate source for geopolymerisation.

The chemical composition determined through X-ray fluorescence (XRF) analysis of the basalt rock fines and ground granulated blast furnace slag is presented in Table.1 which shows that the basalt rock fines are composed mainly of aluminosilicate compounds i.e. silica, SiO_2 = 51.15%, aluminium oxide, Al_2O_3 = 15.89% and calcium oxide, CaO = 7% by mass. In contrast, the ground granulated blast furnace slag composition showed a high percentage of calcium oxide, CaO = 42.71% which indicates that GGBFS is highly reactive and can assist in the enhancement of calcium aluminate silicate hydrate (C-A-S-H) gel linkages, therefore contributing to the formation of a strong geopolymeric gel.

2.3 Mix design ratios

A total of 27 samples were prepared in the first phase of geopolymer mix preparation. Different combinations of varying parameters such as molarity (M) of sodium hydroxide solution, sodium silicate to sodium hydroxide ratio (R) and alkaline activator solution to basalt fines ratio were taken into consideration while preparing the test matrix as shown in Table 2. In the first phase of geopolymer mix preparation, the sodium hydroxide (NaOH) solutions were prepared at different molar concentrations (M) such as 4M, 8M and 12M to investigate the effect of concentration of alkali activator. Several past studies have reported using sodium

187 hydroxide solutions with molarities ranging from 2M to 14M for fly-ash and slag based
188 geopolymers (Görhan and Kürklü, 2014; Jafari Nadoushan and Ramezanianpour, 2016; Lahoti
189 et al., 2017; Laskar and Talukdar, 2017; Lee et al., 2019; Nath and Kumar, 2019; Reddy et al.,
190 2013; Williamson and Juenger, 2016). In this study, 4, 8 and 12M solutions were selected
191 because they cover a wide range of molar concentrations for which maximum efficiency in
192 geopolymerization process and larger strength gains are achieved.

193 To evaluate the role of the sodium silicate (Na_2SiO_3) to sodium hydroxide (NaOH)
194 solutions weighted ratios (R) in the geopolymer strength, specimens having different ratios (i.e.
195 0.25, 0.5 and 1.0) were tested. The sodium hydroxide solution was kept at ambient conditions
196 for 24 hours to achieve equilibrium (Lahoti et al., 2018; Mehta and Siddique, 2017). The alkali
197 activator solution to basalt fines ratio was kept constant at 0.135. This value was selected
198 because it corresponds to the optimum moisture content for basalt fines, whereas the quantity
199 of binder solids was maintained as per the maximum dry unit weight. A summary of the tests
200 conducted in the first phase is shown in Table 2.

201 The main objective was to determine the optimum synthesis parameters for the
202 preparation of basalt fines geopolymer. As the unconfined compressive strength obtained for
203 the specimens prepared in the first phase was smaller (i.e. around 2 MPa) than more established
204 geopolymers, partial replacement with a richer aluminosilicate source (e.g. ground granulated
205 blast furnace slag) was considered. In the second phase, the basalt fines were partially replaced
206 at 10, 20 and 30% by mass with ground granulated blast furnace slag and 81 specimens were
207 prepared as shown in Table 3.

208

209

210

211 *2.4 Specimen preparation and curing*

212 In the first phase, the sodium silicate and sodium hydroxide solutions were mixed in a
213 glass beaker at specific ratios (R), i.e. 0.25, 0.5 and 1.0 for about 30 to 40 minutes. The solution
214 prepared was then added to the basalt fines at the ratios mentioned in Table 2 and mixed for 5
215 to 7 minutes to ensure homogeneous mixing. Cylindrical specimens, 38 mm in diameter and
216 76 mm in height were prepared in steel moulds and compacted statically in 3 layers using a
217 compression frame as per the max dry density i.e. 18.8kN/m^3. Triplicate specimens were
218 prepared for each specific ratio to ensure repeatability of results.

219 Once compacted, the specimens prepared were then wrapped in polyethylene films,
220 sealed in polyethylene resealable bags, and cured at ambient conditions for the required
221 duration under relatively constant temperature (approximately 22°C) and humidity
222 (approximately 95%). Similar procedure was carried out for the specimen preparation in the
223 second phase as per the mix design ratios mentioned in Table 3.

224

225 *2.5 Unconfined compressive strength tests*

226 The basalt fines geopolymer specimens prepared in the first phase were tested for
227 unconfined compressive strength at 7 days. The tests were carried out in accordance with AS
228 5101.4-2008 using Instron 30 kN universal testing machine adopting a strain rate of 0.5
229 mm/min. In the second phase, when the basalt rock fines were partially replaced with ground
230 granulated blast furnace slag (GGBFS), the tests were carried out using 500 kN Instron
231 universal testing machine adopting the same strain rate to avoid any rate dependency effects.
232 The measurement accuracy of the load cell and deformation transducers of both testing systems
233 used was 0.01 N and 0.01 μm, respectively.

234

3. Results and discussion

3.1 Effect of molar concentration of alkali activator solution

The alkaline activator concentration plays a major role in the reactivity, pore microstructure, aluminosilicate gel matrix formation as well as other mechanical properties of geopolymers (Ma et al., 2012; Rashad and Zeedan, 2011; Ruiz-Santaquiteria et al., 2012). The effect for the molar concentration (M) of the sodium hydroxide solution was investigated for the basalt fines geopolymer as well as for the basalt and ground granulated blast furnace slag geopolymer mixes. From the findings of the initial trial mixes, it was observed that the unconfined compressive strengths (UCS) of the basalt fines geopolymer increased with increase in molarity (M) of sodium hydroxide activator from 4M to 8M, for all sodium silicate to sodium hydroxide ratios (R). For instance, for the specimens with sodium silicate to sodium hydroxide ratio (R) of 0.25, the UCS values increased from 0.81 MPa to 1.25 MPa as the molarity of alkali activation solution was increased from 4M to 8M. However, a drop in UCS value to 1.05 MPa was observed when the molarity was increased further to 12M as shown in Figure 5. While these results may not be intuitive at first sight, they are consistent with the results reported in past studies for other geopolymer sources, in which a decrease in compressive strengths beyond optimum value of alkaline concentration was attributed to increased viscosity of activator solution and the presence of unreacted silica and alumina (Barbosa et al., 2000; Hardjito et al., 2008; Jafari Nadoushan and Ramezanianpour, 2016; Williamson and Juenger, 2016).

This is likely associated with the fact that higher molarity favours better reactivity with the aluminosilicate source but only up to an optimum value of 8M. This indicates that the aluminosilicate content would exhibit a higher extent of dissolution to complete the process of geopolymerisation. Once an optimum value is exceeded, the precipitation of dissolved species

inhibits geopolymerisation. For the second phase, the basalt fines and GGBFS geopolymer mixes were tested with 8M and 12M concentrations of the sodium hydroxide solution as 4M concentration was not found sufficient to facilitate the dissolution process.

Figure 6 (a) shows the change in peak compressive stresses of the basalt rock waste and ground granulated blast furnace slag geopolymer prepared using 8M and 12M NaOH concentrations, Na_2SiO_3/NaOH ratio of 0.25 and different slag percentages. It can be seen that as the molarity of NaOH solution increased from 8M to 12M, the compressive strength of the geopolymer specimens decreased. For instance, the compressive strength of 8M-0.25R-10%BFS sample was 11.1 MPa and dropped to 7.9 MPa for 12M-0.25R-10%BFS. Similar trend was observed for all the specimens prepared with varying slag content. This is due to the reason that molarities higher than the optimum value can hinder the complete geopolymeric gel formation. (Görhan and Kürklü, 2014; Jafari Nadoushan and Ramezanianpour, 2016; Williamson and Juenger, 2016).

Figure 6 (b) shows the normalised compressive stress-axial strain behaviour of basalt rock waste and ground granulated blast furnace slag geopolymer prepared using 8M and 12M NaOH concentrations, Na_2SiO_3/NaOH ratio of 0.25 with varying slag content. It can be seen that the 8M specimens exhibited higher strains at peak axial stresses and the values dropped as the molarity of NaOH solution increased to 12M. Further, the 8M specimens for all the varying slag percentages failed in a brittle manner showing a vertical drop in the post-peak curve, whereas the 12M specimens revealed a more ductile behaviour. This could be due to the formation of a monolithic geopolymer gel related to the complete geopolymerisation of the aluminosilicate source at 8M concentration of sodium hydroxide solution. As the material became stiffer at 8M concentrations, it tended to be more brittle whereas the incomplete reactions and free silica in the system at 12M concentration samples resulted in a more ductile

behaviour. Furthermore, 12M samples were found to set quicker probably due to accelerated geopolymerisation reactions, which hindered the compaction process and workability.

The ductility (μ) of geopolymer specimens was calculated using Eq. (1) shown below.

$$\mu = \frac{\varepsilon_2}{\varepsilon_1} \quad (1)$$

The same method has been used for analysing the ductility of geopolymer concrete by various researchers (Ali et al., 2020; Reed et al., 2014). The strain ε_1 represents the value when a tangent to the ascending branch of the stress-strain curve touches the horizontal line at the peak stress and ε_2 shows the strain level at 85% of peak stress value on the descending branch of the curve as shown in Figure 7 (a). As the molarity of specimens increased from 8M to 12M, due to inhibited geopolymerisation process, the gel formed was weaker and thus the ductility of the samples increased. For instance, the ductility of 12M-0.25R-10%BFS was increased by almost 29% as compared to 8M-0.25R-10%BFS. Similar trends were witnessed for all specimens having different slag percentages as shown in Figure 7 (b).

Based on the results reported herein, the optimal molarity of sodium hydroxide solution (M) for the basalt fines geopolymer as well as basalt fines and ground granulated blast furnace slag geopolymer was found to be 8.0 M.

3.2 Effect of sodium silicate to sodium hydroxide ratio

The role of sodium silicate to sodium hydroxide ratios (R) was studied for both basalt fines as well as the basalt and blast furnace slag based geopolymers. From the initial mixes, it was found that the UCS values increased with the increase in the sodium silicate to sodium hydroxide ratios (R) from 0.25 to 1.0R. For instance, for 8M solution, the UCS values were found to be 1.25 MPa at 0.25R, then increased to 1.65 MPa at 0.5R and further increased to

306 around 2.25 MPa for 1.0R, as shown in Figure 8. However, for the mixes with R=1.0, a reduced
307 workability was detected due to accelerated reactions, thus making the mixtures difficult to
308 compact. Figure 9 (a), 9 (b) and 9 (c) illustrate the stress-strain curves for basalt fines and blast
309 furnace slag geopolymer with 8M NaOH concentration and Na_2SiO_3/NaOH ratio (R) of 0.25,
310 0.5 and 0.75 respectively.

311 It was observed that the unconfined compressive strength values increased with the
312 increase of these ratios for 8M concentrations of sodium hydroxide solutions as well as for the
313 samples with 12M concentration of sodium hydroxide shown in Figure 10 (a), 10 (b) and 10
314 (c). For instance, the peak axial stress value for 8M-0.25R-30% BFS specimens was 21 MPa,
315 increased to 32 MPa for 0.5R and further increased to 34 MPa for 0.75R ratios. The peak axial
316 stress value for 12M-0.25R-10% BFS samples was about 7 MPa, increased to 8.2 MPa for 0.5R
317 and further increased to 9.4 MPa for 0.75R ratios. The peak axial stress value for 12M-0.25R-
318 20% BFS samples was 12.5 MPa, increased to 15.1 MPa for 0.5R and further reached 19.4
319 MPa against 0.75R. The peak axial stress value for 12M-0.25R-30% BFS samples was 17.5
320 MPa, increased to 18.7 MPa for 0.5R and further reached 20.4 MPa against 0.75R. The elastic
321 moduli of all the samples increased with the increasing sodium silicate to sodium hydroxide
322 ratios.

323 This trend is consistent with the results reported for geopolymers developed from other
324 established source materials where the increase in R values have contributed to increase in
325 compressive strengths (Paija et al., 2020). However, it was also observed that with the increase
326 in R values, the workability for compaction of samples decreased. The samples with the R
327 value 0.25 were relatively easier to compact. As the values increased to 0.5 and then 0.75, the
328 rate of geopolymerisation was accelerated due to higher content of sodium silicate solution
329 causing earlier setting of the mix, thus making it difficult to compact.

330 Based on the results reported herein, the optimal ratio of sodium silicate to sodium
331 hydroxide solution (R) for the basalt fines geopolymer as well as basalt fines and ground
332 granulated blast furnace slag geopolymer was found to be 0.75.

333

334 *3.3 Effect of silicon to aluminium (Si/Al) ratio*

335 Along with other synthesis parameters, the silicon to aluminium (Si/Al) molar ratio of
336 the geopolymer influences the mechanical strength characteristics of geopolymeric materials.
337 To evaluate the optimum ratio for the aluminosilicate sources considered in this study, i.e. the
338 basalt fines and ground granulated blast furnace slag, geopolymer samples were also prepared
339 in different Si/Al ratios (2.81, 2.91 and 3.10) and their 7-day unconfined compressive strengths
340 were investigated. Figure 11 shows that the peak axial strength values decreased with
341 increasing Si/Al ratios (21 MPa for 2.81, 19MPa for 2.91 and 17 MPa for 3.10). This is likely
342 caused by the higher quantity of unreacted silica present in the system. Another contributing
343 factor could be increased viscosity of the alkali solution contributing to inhomogeneous mixing
344 and a more porous structure.

345 In the past, optimum ratios have been determined for geopolymers based on various
346 natural and industrial waste sources (He et al., 2016; Lahoti et al., 2018; Lizcano et al., 2012;
347 Timakul et al., 2015). The optimum Si/Al ratio investigation for metakaolin and fly ash based
348 geopolymers (Asif et al., 2015; Lizcano et al., 2012; Thokchom et al., 2012; Timakul et al.,
349 2015) revealed that as the Si/Al ratios tend to reach closer to 3.0, the strength values for that
350 geopolymer mix would be lowered as reported in the past literature and shown in Table 4. The
351 novel basalt and slag based geopolymer proposed in this study follows a similar principle of
352 currently existing metakaolin, fly-ash and slag based geopolymers thus confirming its potential
353 usage as an alternative cementitious material to be considered in construction industry.

354 *3.4 Effect of ground granulated blast furnace slag (GGBFS)*

355 The strength gain in many geopolymer materials is occasionally slow due to lack of
356 calcium content in various precursors, which may result in a larger setting time (Cho et al.,
357 2017). In such conditions, addition of high calcium additives such as ground granulated blast
358 furnace slag can assist in accelerating the chemical reactions and facilitate the attainment of
359 high early strength (Chindaprasirt et al., 2011; Deb et al., 2014). The basalt content in the
360 geopolymer precursor mix was partially replaced by 10, 20 and 30% by mass to analyse the
361 compressive strength behaviour. Figure 12 shows the stress strain behaviour of basalt
362 geopolymer prepared at 8M NaOH concentration and Na_2SiO_3/NaOH ratio of 0.75 with
363 varying levels of blast furnace slag. As expected, the peak axial stresses increase for higher
364 content of blast furnace slag i.e. 11 MPa, 28 MPa and 34 MPa for 10, 20% and 30%
365 replacement, respectively. The Young's moduli also increased with the increase in percentage
366 of ground granulated blast furnace slag. The values increased with higher content of blast
367 furnace slag i.e. 2.65 GPa, 3.47 GPa and 4.30 GPa for 10, 20% and 30% replacement,
368 respectively.

369 Figure 13 shows a comparison chart of compressive strength of basalt fines geopolymer
370 with 8M NaOH concentration and various Na_2SiO_3/NaOH ratios at different percentages of
371 GGBFS. As expected, an increase in strength was observed in the specimens having higher
372 percentage of GGBFS. For instance, for all the different R ratios considered, specimens having
373 a larger GGBFS replacement percentage exhibited larger compressive strengths, often resulting
374 in an increase of over 15MPa (e.g. 8M – 0.5R and 8M – 0.75R) for an increase from 10% to
375 30% replacement of GGBFS. This is likely associated with the accelerated geopolymerisation
376 reactions which are facilitated by calcium content in the system derived from higher percentage
377 of GGBFS. This in turn led to the formation of a denser, monolithic and a less porous
378 microstructure geopolymer which achieved high early compressive strengths. These results

show that the proposed geopolymer could prove to be a promising alternative to already established geopolymers while adding value to the product that is being currently landfilled. However, some workability issues could arise due to the decrease in setting time, which may require some further research.

Considering the strength, workability and microstructure characteristics reported in previous sections, the minimum GGBFS replacement percentage required to achieve comparable performance to more established geopolymers is 30%. However, it should be noted that smaller replacement percentages may be considered for applications where compressive strengths exceeding 30 MPa are not required.

3.5 Effect of aging

Figure 14 shows the stress-strain behaviour for basalt fines and 30 % blast furnace slag geopolymer with respect to curing time or aging. As expected, larger peak axial stresses and Young's moduli were achieved for specimens having more curing time, however the rate of change varied considerably in the first week (Figure 15). For instance, the peak axial stresses increased from 15.5 MPa (1 day) to 34.2 MPa (7 days) whereas the Young's moduli increased from 1.70 GPa (1 day) to 5.60 GPa (7 days) during the first week. After the first 7 days, the increase in the peak axial stresses was slower. The peak axial stress at 28 days was 42 MPa while the Young's modulus rose to 6.08 GPa. The variation in compressive strengths of basalt fines and 30% blast furnace slag geopolymer with respect to time is shown in Figure 15.

The gain in strength is drastic in the first 7 days and reaches 34.2 MPa at an average of 4.88 MPa per day. This is possibly due to the geopolymeric chains being formed in the early curing after which the material hardens and the rate of strength gain decreases to an average of 0.38 MPa per day reaching a 28 day strength of 42 MPa. This rapid gain in strength in the first

403 week allows the basalt and slag based geopolymer to be used as a promising material where
404 high early compressive strengths are desired. Typically, the strength gain of geopolymers
405 occurs at a much lower rate after 7 days (Deb et al., 2014; Khale and Chaudhary, 2007). This
406 behaviour was confirmed by the scanning electron microscopy (SEM) images, which showed
407 that the microstructure of basalt fines and blast furnace slag geopolymer in the 7 day and 28
408 day exhibited similarity.

409

410 *3.6 Microstructure analysis*

411 The scanning electron microscopy (SEM) micrographs were taken for both basalt fines
412 as well as basalt fines-blast furnace slag geopolymers. Figure 16 shows the SEM micrographs
413 for basalt fines geopolymer at different molar concentrations of sodium hydroxide activator
414 solution. It can be observed that as the molarity of the alkaline solution increased from 4M to
415 12M, it enhanced the dissolution of silica particles in the gel matrix, thus reducing the amount
416 of free silica due to consumption in the geopolymerisation reaction. As a result, the gel becomes
417 denser and the material exhibits higher compressive strength.

418 The SEM micrographs for basalt fines geopolymer with partial replacement of basalt
419 dust with 10, 20 and 30% of ground granulated blast furnace slag are illustrated in Figure 17.
420 It is evident from the images that as the GGBFS content increases from 10 to 30%, the larger
421 amount of reactive calcium in the system results in a denser microstructure. The gel formed is
422 monolithic in nature and the pore size is estimated to be reduced to around 3µm as compared
423 to the 9µm exhibited in the original basalt fines microstructure. Figure 18 shows the SEM
424 micrographs of basalt fines and 30% blast furnace slag geopolymer (8M-0.75R-30%BFS in
425 particular) at 7 days and 28 days, respectively. It is observed that a well compacted and dense
426 gel formation occurs in the first seven days of geopolymerisation when the material has

undergone most of the chemical reactions and entered into its hardening stage. After the first week, the geopolymer gel gains strength at a much lower rate. This phenomenon is confirmed from the SEM images at 28 days of formation, as significant difference in the geopolymer gel is not observed also at the microstructure level. The microstructural characteristics of this new basalt and ground granulated blast furnace slag based geopolymer substantiate that the geopolymeric gel development mechanism and behaviour of this material is comparable to already established geopolymers from other precursor sources (Duxson et al., 2007; Izquierdo et al., 2009; Ma et al., 2013; Schmücker and MacKenzie, 2005) thus validating its potential application as a supplementary cementitious material.

4. Cost Analysis

One of the major factors contributing to the usage of any material in the construction industry is its cost. In this study, quotations from different supplier companies such as PQ Corporation Australia, Bondall Australia, Boral Australia and Australasian Slag Association were obtained in order to carry out cost analysis. The average cost of some conventional precursor materials used in the synthesis of geopolymers are for instance, fly-ash costs AU$ 600/ton, metakaolin around AU$ 550/ton and GGBFS around AU$ 80/ton. The alkaline activator like sodium hydroxide solution can cost around AU$ 9000/ton whereas sodium silicate solution may cost around AU$ 6500/ton. Using basalt dust waste and ground granulated blast furnace slag (GGBFS) geopolymer in the mix proportions suggested above, the per cubic meter cost will range from AU$ 1000 to AU$ 1200 thus reducing the cost by up to 50% as compared to conventional fly-ash based geopolymers. It should be noted that the cost exercise presented here is an example and assumes the raw materials are readily available in the vicinity of where the geopolymer is being produced. In contrast, in more remote locations where

quarried fines waste may not be available, the cost of transport may tip decision towards the use of more established precursors materials. Thus, a detailed analysis should be undertaken on a project to project basis.

5. Conclusions

In this study, an attempt was made to utilise basalt rock fines currently categorised as landfill wastes from quarry sites in combination with steel industry waste by-product, i.e., ground granulated blast furnace slag to develop a series of new geopolymer mixes suitable for usage as an alternative, environment-friendly construction material. The main conclusions that can be drawn from this study are summarised as follows.

1. While the geopolymer based on basalt fines alone has shown potential, the compressive strengths obtained were small (around 2 MPa) compared to other conventional geopolymers developed from metakaolin, fly-ash etc. (30-50 MPa).
2. An addition of a richer aluminosilicate source, i.e. partial replacement up to weight ratios of 30% of ground granulated blast furnace slag (GGBFS), has enhanced the mechanical properties of the geopolymer mixes obtained and unconfined compressive strengths (UCS) up to 34 MPa were achieved with varying GGBFS ratios.
3. The optimum molarity (M) of the sodium hydroxide activator solution was found to be 8M whereas the optimum weighted ratio of the sodium silicate to sodium hydroxide solution (R) was found to be 0.75. The experimental results revealed that the compressive strength values would increase even at higher ratios but at the cost of workability of the geopolymer mix. At values more than 0.75, the chemical reactions are accelerated which result in the decrease in setting time of the mix, thus making the samples difficult to compact. Sodium silicate is one of the major components of

geopolymers contributing towards strength; however, it also significantly results in excessive greenhouse gas emissions. Although higher ratios (approximately 2.5) have been utilised in geopolymer concrete production in literature, the lower ratios in this innovative basalt and slag based geopolymer mix can prove to reduce the carbon footprint as well as the production cost.

4. The basalt and GGBFS geopolymer prepared showed 7 days compressive strengths up to 34.2 MPa and exhibited a slower strength gain up to 28 days curing (i.e. maximum peak strength of 42 MPa). The SEM micrographs revealed that the microstructure developed in the first week was highly monolithic, dense with a reduced pore size, therefore contributing to high early strengths.
5. The basalt and GGBFS geopolymer prepared shows a reduction in cost by up to 50% and may prove to be a cost effective alternative to alkali-activated geopolymers prepared from other conventional precursors such as metakaolin and fly ash.

In light of the above, the proposed basalt rock fines and GGBFS based geopolymer can prove to be a value added product having a potential usage as an alternative cementitious material in the construction industry. The utilisation of landfill and industrial waste products such as the ones used in this research can act as a major step towards greener construction practices.

Acknowledgements

The authors gratefully acknowledge the financial assistance for the first author from a joint scholarship program by Higher Education Commission (Pakistan) through the Human Resource Development Initiative - Faculty Development Program and the University of

Wollongong, Australia. Laboratory assistance by Mr. Richard Berndt and Mr. Duncan Best is highly appreciated. Assistance provided with the procurement of materials from local quarries, PQ Australia and Australasian Slag Association (ASA) is also hereby recognized.

CRediT Author statement

The paper is a joint contribution of all authors but specific contributions can be recognised as follows,

Mohsin Nawaz: Methodology, Laboratory experiments, Writing - Original Draft,

Ana Heitor: Conceptualization, Writing - Review & Editing, Resources, Supervision, Project administration

Muttucumaru Sivakumar: Conceptualization, Writing - Review & Editing, Resources, Supervision

Declaration of Interest Statement

The authors declare that they have no known competing financial interests or personal relationships that could have appeared to influence the work reported in this paper.

6. References

Ahmad, J., Ali, S., Yu, T., Sheikh, M.N., Hadi, M.N.S., 2021. Analytical investigation on the load-moment interaction behavior of the FRP reinforced geopolymer concrete filled FRP tube circular columns. Journal of Building Engineering 42, 102818.

Akbar, A., Farooq, F., Shafique, M., Aslam, F., Alyousef, R., Alabduljabbar, H., 2021. Sugarcane bagasse ash-based engineered geopolymer mortar incorporating propylene fibers. Journal of Building Engineering 33, 101492.

Ali, S., Sheikh, M.N., Sargeant, M., Hadi, M.N.S., 2020. Influence of Polypropylene and Glass Fibers on Alkali- Activated Slag/Fly Ash Concrete. ACI Structural Journal 117(4).

Andrew, R.M., 2018. Global CO2 emissions from cement production, 1928–2017. Earth Syst. Sci. Data 10(4), 2213-2239.

Arulrajah, A., Kua, T.-A., Suksiripattanapong, C., Horpibulsuk, S., Shen, J.S., 2017. Compressive strength and microstructural properties of spent coffee grounds-bagasse ash based geopolymers with slag supplements. Journal of Cleaner Production 162, 1491-1501.

Asif, A., Man, Z., Mohd Azizli, K.A., Nuruddin, M.F., Ismail, L., 2015. The Effect of Si/Al Ratio and Sodium Silicate on the Mechanical Properties of Fly Ash Based Geopolymer for Coating. Materials Science Forum 803, 355-361.

Azevedo, A.R.G., Vieira, C.M.F., Ferreira, W.M., Faria, K.C.P., Pedroti, L.G., Mendes, B.C., 2020. Potential use of ceramic waste as precursor in the geopolymerization reaction for the production of ceramic roof tiles. Journal of Building Engineering 29, 101156.

Barbosa, V.F.F., MacKenzie, K.J.D., Thaumaturgo, C., 2000. Synthesis and characterisation of materials based on inorganic polymers of alumina and silica: Sodium polysialate polymers. International Journal of Inorganic Materials 2(4), 309-317.

Chindaprasirt, P., Chareerat, T., Hatanaka, S., Cao, T., 2011. High-Strength Geopolymer Using Fine High-Calcium Fly Ash. Journal of Materials in Civil Engineering 23(3), 264-270.

Chindaprasirt, P., Chareerat, T., Sirivivatnanon, V., 2007. Workability and strength of coarse high calcium fly ash geopolymer. Cement and Concrete Composites 29(3), 224-229.

Cho, Y.-K., Yoo, S.-W., Jung, S.-H., Lee, K.-M., Kwon, S.-J., 2017. Effect of Na2O content, SiO2/Na2O molar ratio, and curing conditions on the compressive strength of FA-based geopolymer. Construction and Building Materials 145, 253-260.

Davidovits, J., 1989. Geopolymers and geopolymeric materials. Journal of thermal analysis 35(2), 429-441.

Deb, P.S., Nath, P., Sarker, P.K., 2014. The effects of ground granulated blast-furnace slag blending with fly ash and activator content on the workability and strength properties of geopolymer concrete cured at ambient temperature. Materials & Design (1980-2015) 62, 32-39.

Duxson, P., Fernández-Jiménez, A., Provis, J.L., Lukey, G.C., Palomo, A., Van Deventer, J.S.J., 2007. Geopolymer technology: The current state of the art. Journal of Materials Science 42(9), 2917-2933.

Eliche-Quesada, D., Ruiz-Molina, S., Pérez-Villarejo, L., Castro, E., Sánchez-Soto, P.J., 2020. Dust filter of secondary aluminium industry as raw material of geopolymer foams. Journal of Building Engineering 32, 101656.

Erfanimanesh, A., Sharbatdar, M.K., 2020. Mechanical and microstructural characteristics of geopolymer paste, mortar, and concrete containing local zeolite and slag activated by sodium carbonate. Journal of Building Engineering 32, 101781.

Görhan, G., Kürklü, G., 2014. The influence of the NaOH solution on the properties of the fly ash-based geopolymer mortar cured at different temperatures. Composites Part B: Engineering 58, 371-377.

Hardjito, D., Cheak, C.C., Ing, C.H.L., 2008. Strength and setting times of low calcium fly ash-based geopolymer mortar. Modern Applied Science 2(4), 3-11.

Hardjito, D., Wallah, S.E., Sumajouw, D.M.J., Rangan, B.V., 2005. Fly ash-based geopolymer concrete. Australian Journal of Structural Engineering 6(1), 77-86.

569 Hassan, A., Arif, M., Shariq, M., 2020. A review of properties and behaviour of reinforced geopolymer
570 concrete structural elements- A clean technology option for sustainable development. Journal of
571 Cleaner Production 245, 118762.
572 He, P., Wang, M., Fu, S., Jia, D., Yan, S., Yuan, J., Xu, J., Wang, P., Zhou, Y., 2016. Effects of Si/Al ratio
573 on the structure and properties of metakaolin based geopolymer. Ceramics International 42(13),
574 14416-14422.
575 Hoppe Filho, J., Pires, C.A.O., Leite, O.D., Garcez, M.R., Medeiros, M.H.F., 2021. Red ceramic waste as
576 supplementary cementitious material: Microstructure and mechanical properties. Construction and
577 Building Materials 296, 123653.
578 Izquierdo, M., Querol, X., Davidovits, J., Antenucci, D., Nugteren, H., Fernández-Pereira, C., 2009. Coal
579 fly ash-slag-based geopolymers: Microstructure and metal leaching. Journal of Hazardous Materials
580 166(1), 561-566.
581 Jafari Nadoushan, M., Ramezanianpour, A.A., 2016. The effect of type and concentration of activators
582 on flowability and compressive strength of natural pozzolan and slag-based geopolymers.
583 Construction and Building Materials 111, 337-347.
584 Khale, D., Chaudhary, R., 2007. Mechanism of geopolymerization and factors influencing its
585 development: a review. Journal of Materials Science 42(3), 729-746.
586 Kolovos, K.G., Asteris, P.G., Cotsovos, D.M., Badogiannis, E., Tsivilis, S., 2013. Mechanical properties of
587 soilcrete mixtures modified with metakaolin. Construction and Building Materials 47, 1026-1036.
588 Kwasny, J., Aiken, T.A., Soutsos, M.N., McIntosh, J.A., Cleland, D.J., 2018. Sulfate and acid resistance
589 of lithomarge-based geopolymer mortars. Construction and Building Materials 166, 537-553.
590 Lahoti, M., Wong, K.K., Tan, K.H., Yang, E.-H., 2017. Use of alkali-silica reactive sedimentary rock
591 powder as a resource to produce high strength geopolymer binder. Construction and Building
592 Materials 155(Supplement C), 381-388.
593 Lahoti, M., Wong, K.K., Yang, E.-H., Tan, K.H., 2018. Effects of Si/Al molar ratio on strength endurance
594 and volume stability of metakaolin geopolymers subject to elevated temperature. Ceramics
595 International 44(5), 5726-5734.
596 Laskar, S.M., Talukdar, S., 2017. Preparation and tests for workability, compressive and bond strength
597 of ultra-fine slag based geopolymer as concrete repairing agent. Construction and Building Materials
598 154, 176-190.
599 Lee, W.-H., Wang, J.-H., Ding, Y.-C., Cheng, T.-W., 2019. A study on the characteristics and
600 microstructures of GGBS/FA based geopolymer paste and concrete. Construction and Building
601 Materials 211, 807-813.
602 Lizcano, M., Kim, H.S., Basu, S., Radovic, M., 2012. Mechanical properties of sodium and potassium
603 activated metakaolin-based geopolymers. Journal of Materials Science 47(6), 2607-2616.
604 Ma, Y., Hu, J., Ye, G., 2012. The effect of activating solution on the mechanical strength, reaction rate,
605 mineralogy, and microstructure of alkali-activated fly ash. Journal of Materials Science 47(11), 4568-
606 4578.
607 Ma, Y., Hu, J., Ye, G., 2013. The pore structure and permeability of alkali activated fly ash. Fuel 104,
608 771-780.
609 Malkawi, A.B., Habib, M., Aladwan, J., Alzubi, Y., 2020. Engineering properties of fibre reinforced
610 lightweight geopolymer concrete using palm oil biowastes. Australian Journal of Civil Engineering
611 18(1), 82-92.
612 Mathew, G., Issac, B.M., 2020. Effect of molarity of sodium hydroxide on the aluminosilicate content
613 in laterite aggregate of laterised geopolymer concrete. Journal of Building Engineering 32, 101486.
614 Mehta, A., Siddique, R., 2017. Strength, permeability and micro-structural characteristics of low-
615 calcium fly ash based geopolymers. Construction and Building Materials 141, 325-334.
616 Nath, S.K., Kumar, S., 2019. Role of alkali concentration on reaction kinetics of fly ash
617 geopolymerization. Journal of Non-Crystalline Solids 505, 241-251.
618 Nawaz, M., Heitor, A., Sivakumar, M., 2020. Geopolymers in construction - recent developments.
619 Construction and Building Materials 260, 120472.

Nunes, J.M.G., Kautzmann, R.M., Oliveira, C., 2014. Evaluation of the natural fertilizing potential of basalt dust wastes from the mining district of Nova Prata (Brazil). Journal of Cleaner Production 84, 649-656.
Paija, N., Kolay, P.K., Mohanty, M., Kumar, S., 2020. Ground Bottom Ash Application for Conventional Mortar and Geopolymer Paste. Journal of Hazardous, Toxic, and Radioactive Waste 24(1), 04019025.
Palomo, A., Grutzeck, M.W., Blanco, M.T., 1999. Alkali-activated fly ashes: A cement for the future. Cement and Concrete Research 29(8), 1323-1329.
Phummiphan, I., Horpibulsuk, S., Rachan, R., Arulrajah, A., Shen, S.-L., Chindaprasirt, P., 2018. High calcium fly ash geopolymer stabilized lateritic soil and granulated blast furnace slag blends as a pavement base material. Journal of Hazardous Materials 341, 257-267.
Ramlochan, T., Thomas, M., Gruber, K.A., 2000. The effect of metakaolin on alkali–silica reaction in concrete. Cement and Concrete Research 30(3), 339-344.
Rashad, A.M., Zeedan, S.R., 2011. The effect of activator concentration on the residual strength of alkali-activated fly ash pastes subjected to thermal load. Construction and Building Materials 25(7), 3098-3107.
Reddy, D.V., Edouard, J.-B., Sobhan, K., 2013. Durability of Fly Ash–Based Geopolymer Structural Concrete in the Marine Environment. Journal of Materials in Civil Engineering 25(6), 781-787.
Reed, M., Lokuge, W., Karunasena, W., 2014. Fibre-reinforced geopolymer concrete with ambient curing for in situ applications. Journal of Materials Science 49(12), 4297-4304.
Rios, S., Ramos, C., Viana da Fonseca, A., Cruz, N., Rodrigues, C., 2019. Mechanical and durability properties of a soil stabilised with an alkali-activated cement. European Journal of Environmental and Civil Engineering 23(2), 245-267.
Ruiz-Santaquiteria, C., Skibsted, J., Fernández-Jiménez, A., Palomo, A., 2012. Alkaline solution/binder ratio as a determining factor in the alkaline activation of aluminosilicates. Cement and Concrete Research 42(9), 1242-1251.
Samarakoon, M.H., Ranjith, P.G., Hui Duan, W., Haque, A., Chen, B.K., 2021. Extensive use of waste glass in one-part alkali-activated materials: Towards sustainable construction practices. Waste Management 130, 1-11.
Sata, V., Sathonsaowaphak, A., Chindaprasirt, P., 2012. Resistance of lignite bottom ash geopolymer mortar to sulfate and sulfuric acid attack. Cement and Concrete Composites 34(5), 700-708.
Schmücker, M., MacKenzie, K.J.D., 2005. Microstructure of sodium polysialate siloxo geopolymer. Ceramics International 31(3), 433-437.
Serag Faried, A., Sofi, W.H., Taha, A.-Z., El-Yamani, M.A., Tawfik, T.A., 2020. Mix Design Proposed for Geopolymer Concrete Mixtures Based on Ground Granulated Blast furnace slag. Australian Journal of Civil Engineering 18(2), 205-218.
Shobeiri, V., Bennett, B., Xie, T., Visintin, P., 2021. A comprehensive assessment of the global warming potential of geopolymer concrete. Journal of Cleaner Production 297, 126669.
Sontia Metekong, J.V., Kaze, C.R., Deutou, J.G., Venyite, P., Nana, A., Kamseu, E., Melo, U.C., Tatietse, T.T., 2020. Evaluation of performances of volcanic-ash-laterite based blended geopolymer concretes: Mechanical properties and durability. Journal of Building Engineering, 101935.
Stafford, F.N., Raupp-Pereira, F., Labrincha, J.A., Hotza, D., 2016. Life cycle assessment of the production of cement: A Brazilian case study. Journal of Cleaner Production 137, 1293-1299.
Sturm, P., Gluth, G.J.G., Jäger, C., Brouwers, H.J.H., Kühne, H.C., 2018. Sulfuric acid resistance of one-part alkali-activated mortars. Cement and Concrete Research 109, 54-63.
Thokchom, S., Mandal, K.K., Ghosh, S., 2012. Effect of Si/Al Ratio on Performance of Fly Ash Geopolymers at Elevated Temperature. Arabian Journal for Science and Engineering 37(4), 977-989.
Timakul, P., Thanaphatwetphisit, K., Aungkavattana, P., 2015. Effect of Silica to Alumina Ratio on the Compressive Strength of Class C Fly Ash-Based Geopolymers. Key Engineering Materials 659, 80-84.
Top, S., Vapur, H., 2018. Effect of basaltic pumice aggregate addition on the material properties of fly ash based lightweight geopolymer concrete. Journal of Molecular Structure 1163, 10-17.

671 Wasim, M., Ngo, T.D., Law, D., 2021. A state-of-the-art review on the durability of geopolymer
672 concrete for sustainable structures and infrastructure. Construction and Building Materials 291,
673 123381.
674 Williamson, T., Juenger, M.C.G., 2016. The role of activating solution concentration on alkali–silica
675 reaction in alkali-activated fly ash concrete. Cement and Concrete Research 83, 124-130.
676 Wong, C.L., Mo, K.H., Alengaram, U.J., Yap, S.P., 2020. Mechanical strength and permeation properties
677 of high calcium fly ash-based geopolymer containing recycled brick powder. Journal of Building
678 Engineering 32, 101655.
679 Xie, T., Fang, C., 2019. Nanomaterials Applied in Modifications of Geopolymer Composites: a Review.
680 Australian Journal of Civil Engineering 17(1), 32-49.
681 Xie, T., Visintin, P., Zhao, X., Gravina, R., 2020. Mix design and mechanical properties of geopolymer
682 and alkali activated concrete: Review of the state-of-the-art and the development of a new unified
683 approach. Construction and Building Materials 256, 119380.
684 Zhang, M., Guo, H., El-Korchi, T., Zhang, G., Tao, M., 2013. Experimental feasibility study of geopolymer
685 as the next-generation soil stabilizer. Construction and Building Materials 47, 1468-1478.

686

687

688

689

690

691

692

693

694

695

696

697

698

699

700

701

702

703

704

705

706

List of Tables

738 Table. 1 Chemical composition of basalt rock fines and ground granulated blast furnace slag

739

Component	Basalt fines (mass %)	GGBFS (mass %)
SiO_2	51.15	34.46
Al_2O_3	15.89	12.78
CaO	7.00	42.71
Fe_2O_3	8.37	0.39
Na_2O	3.36	0.75
MgO	2.79	5.32
P_2O_5	0.73	0.08
SO_3	0.11	1.68
K_2O	3.71	0.27
Mn_2O_3	0.18	0.39
TiO_2	1.00	0.82
Loss on Ignition (LOI)	5.42	0.14

740

741

742

743

744

745

746

747

748

749

750

751

752

753

754

755

756

757

758

Table 2. Summary of test matrix for phase-I

Molarity of NaOH (M)	**($NaOH+Na_2SiO_3$)/Basalt (by weight)**	**Na_2SiO_3/NaOH (R) (by weight)**	**Number of specimens**
4M	0.135	0.25	3
	0.135	0.5	3
	0.135	1.0	3
8M	0.135	0.25	3
	0.135	0.5	3
	0.135	1.0	3
12M	0.135	0.25	3
	0.135	0.5	3
	0.135	1.0	3
			Total: 27

776 Table 3. Summary of test matrix for phase-II

777

Molarity of NaOH (M)	Na_2SiO_3/NaOH (R) by mass	GGBFS percentage (%) by mass	No. of Specimens
4	0.25	10	3
		20	3
		30	3
	0.5	10	3
		20	3
		30	3
	0.75	10	3
		20	3
		30	3
8	0.25	10	3
		20	3
		30	3
	0.5	10	3
		20	3
		30	3
	0.75	10	3
		20	3
		30	3
12	0.25	10	3
		20	3
		30	3
	0.5	10	3
		20	3
		30	3
	0.75	10	3
		20	3
		30	3
			Total: 81

778

779

780

781

782 Table 4. Comparison table for effect of Si/Al ratio on strength of geopolymers in past
783 literature

784

Authors	Si/Al ratios	Comments
Asif et al. (2015)	1.85, 2.0, 2.5 and 3.0	The compressive strengths increased till a ratio of 2.0 after which they decreased
Timakul et al. (2015)	2.6, 2.65, 2.8 and 3.0	The compressive strengths increased till a ratio of 2.65 after which a decrease was witnessed
He et al. (2013)	1.68, 2.24, 2.80 and 3.35	The compressive strengths increased till a ratio of 2.80 after which the values lowered
Lizcano et al. (2012)	1.25, 1.5, 2.0 and 2.5	The compressive strengths increased till a ratio of 1.5 after which they decreased
Zhang et al. (2011)	1.89 to 7.78	The compressive strengths were highest for a ratio of 1.89 after which they started to decrease

785

786

787

788

789

790

791

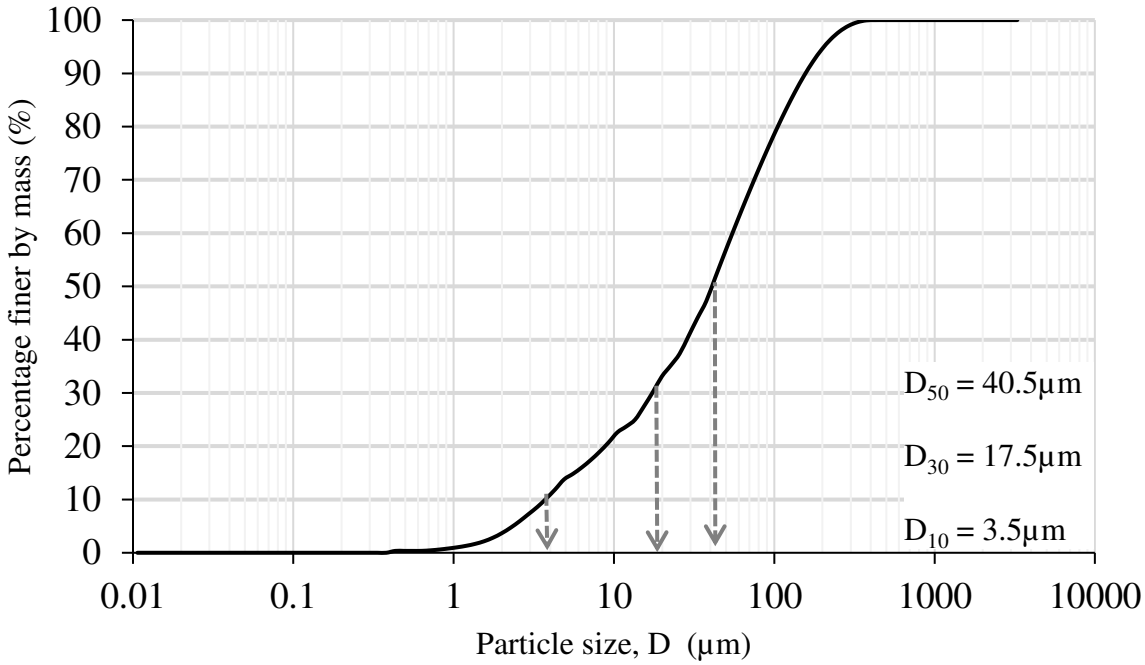

Figure 1 Particle size distribution of basalt fines

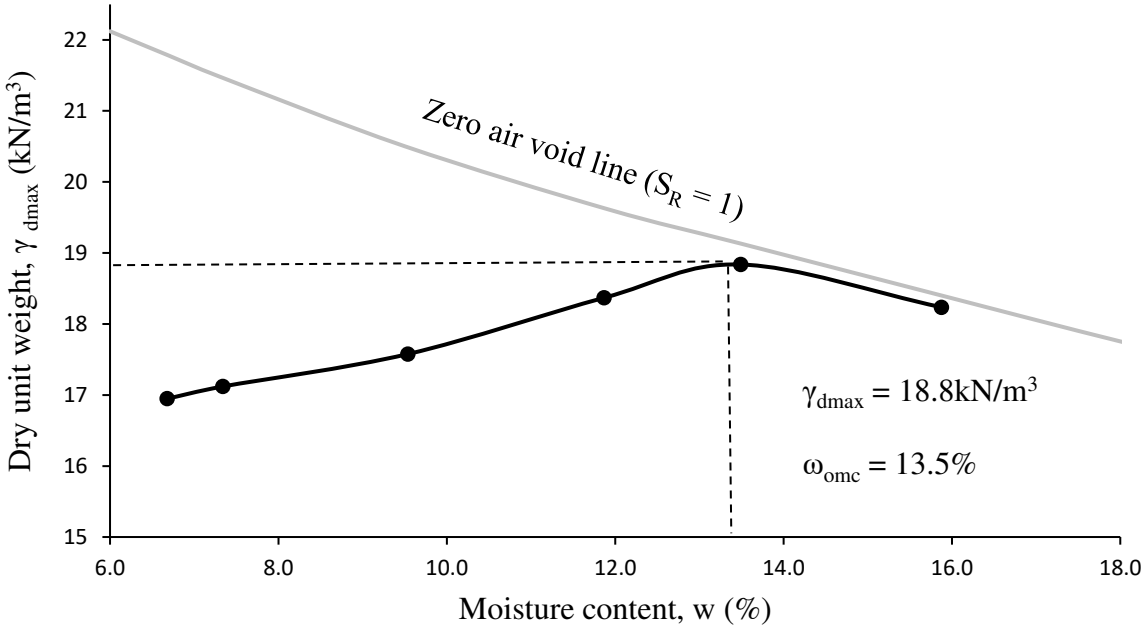

Figure 2 Compaction curve for basalt rock fines

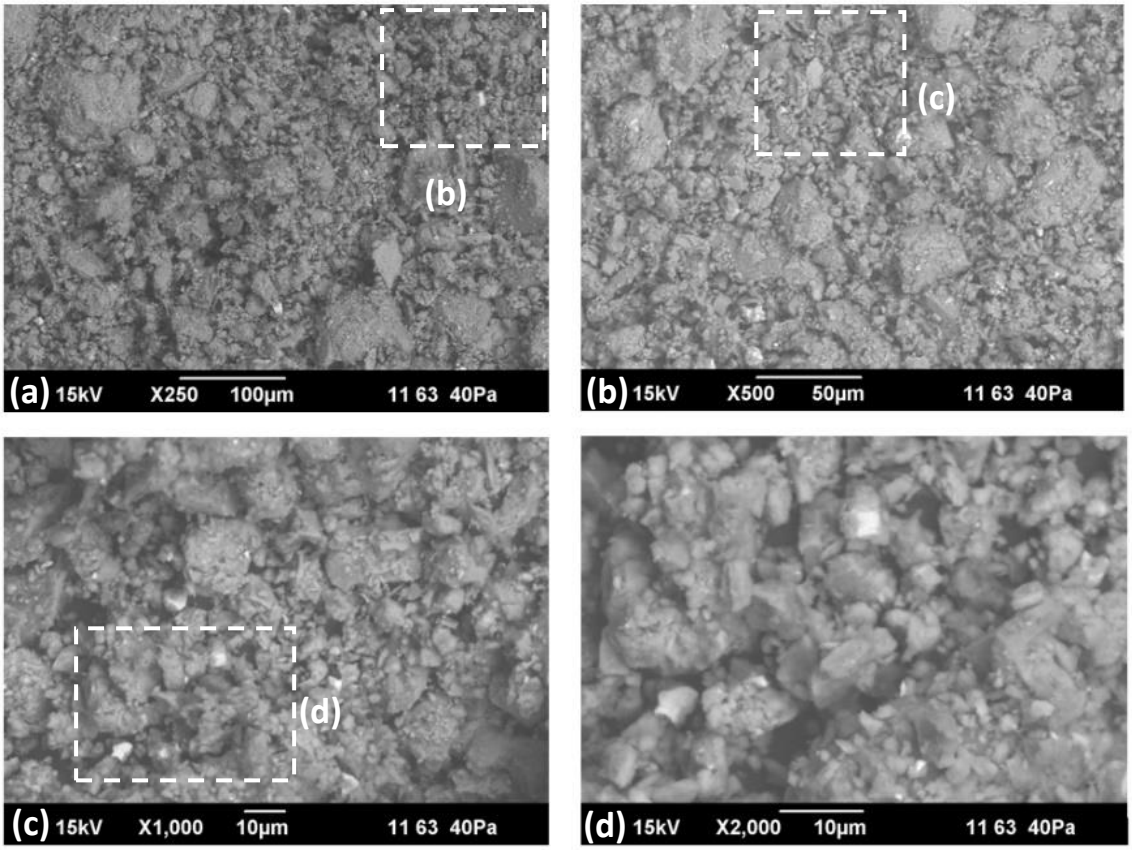

Figure 3 SEM images of basalt fines at various magnifications (a) x250 (b) x500 (c) x1000 and (d) x2000 (Micrographs taken by Mohsin Nawaz) (squares represent the magnified regions)

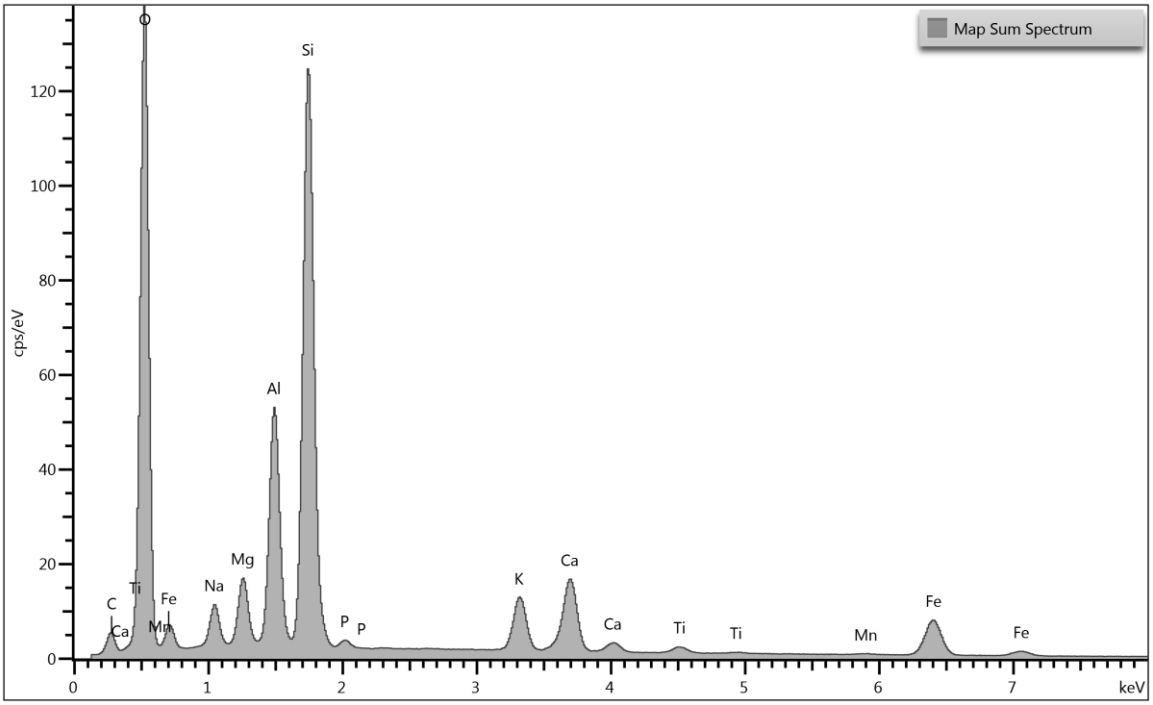

Figure 4 Energy dispersive spectroscopy analysis of basalt fines (average spectrum)

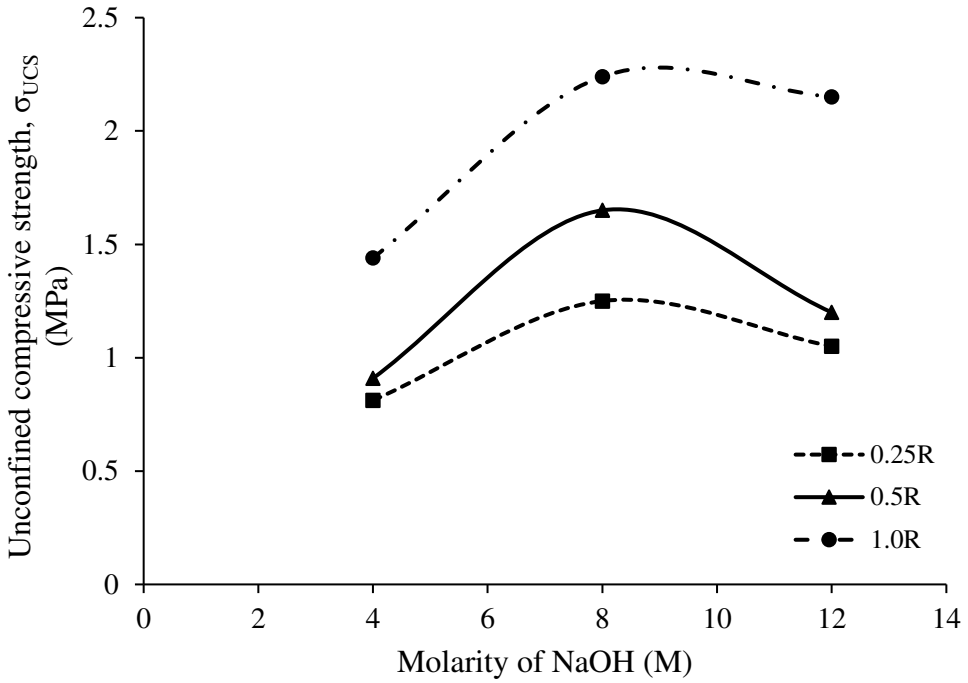

Figure 5 Compressive strength variation for basalt fines geopolymer w.r.t. molarity (M) of NaOH

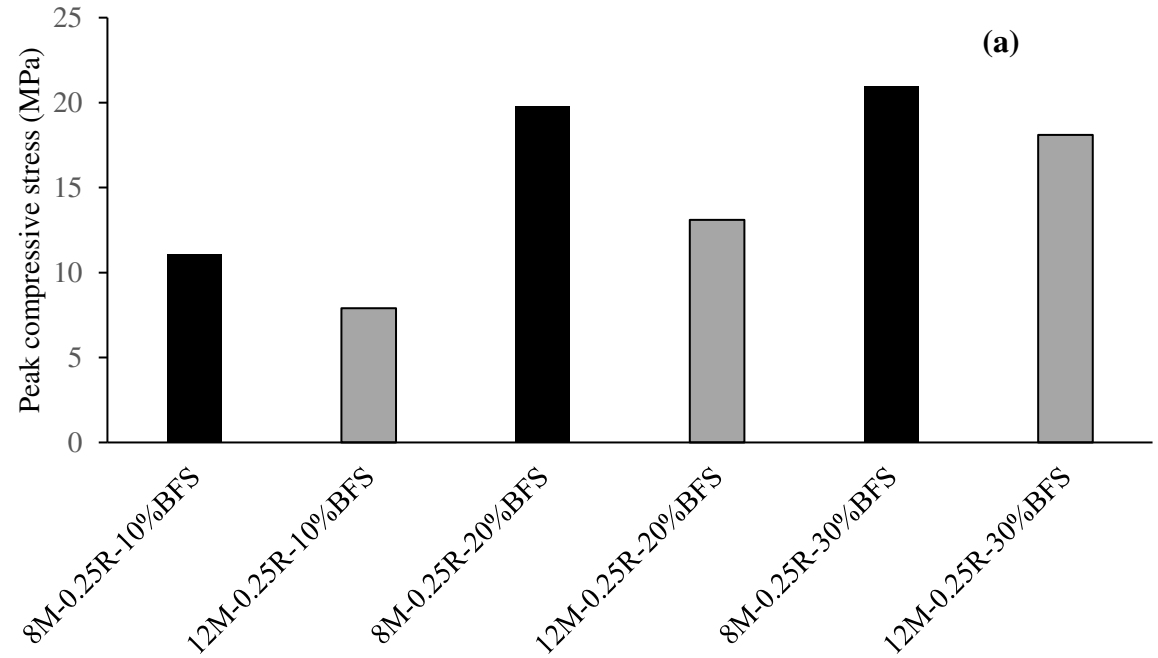

886

887

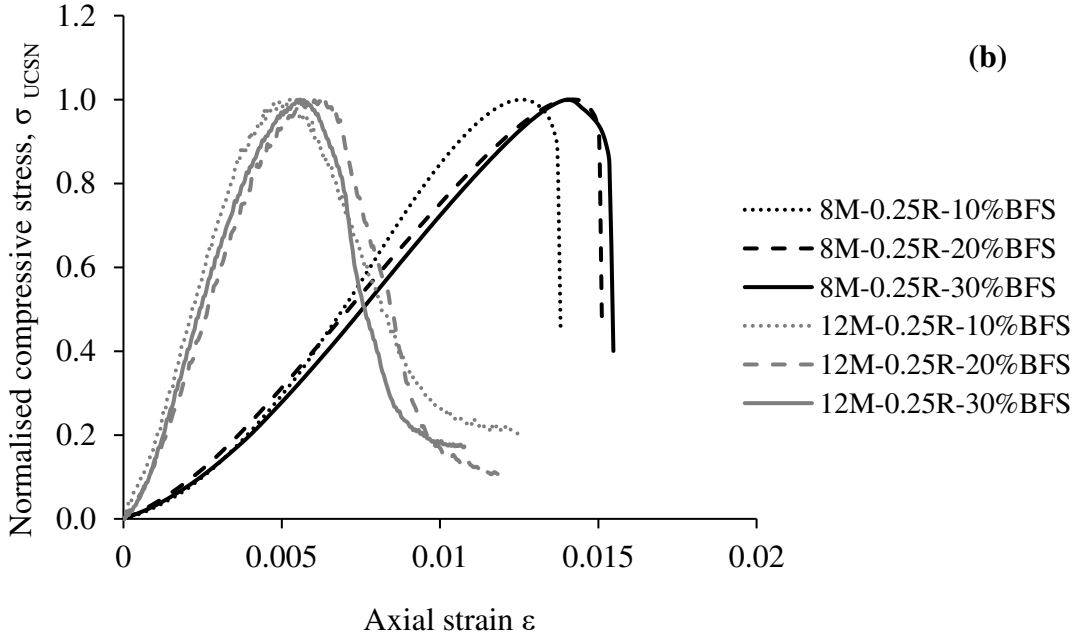

888

889 Figure 6 (a) Peak compressive stress of 8M and 12M geopolymer samples with varying slag
890 content (b) Normalised compressive stress-axial strain behaviour of 8M and 12M geopolymer
891 samples with varying slag content

892

893

894

895

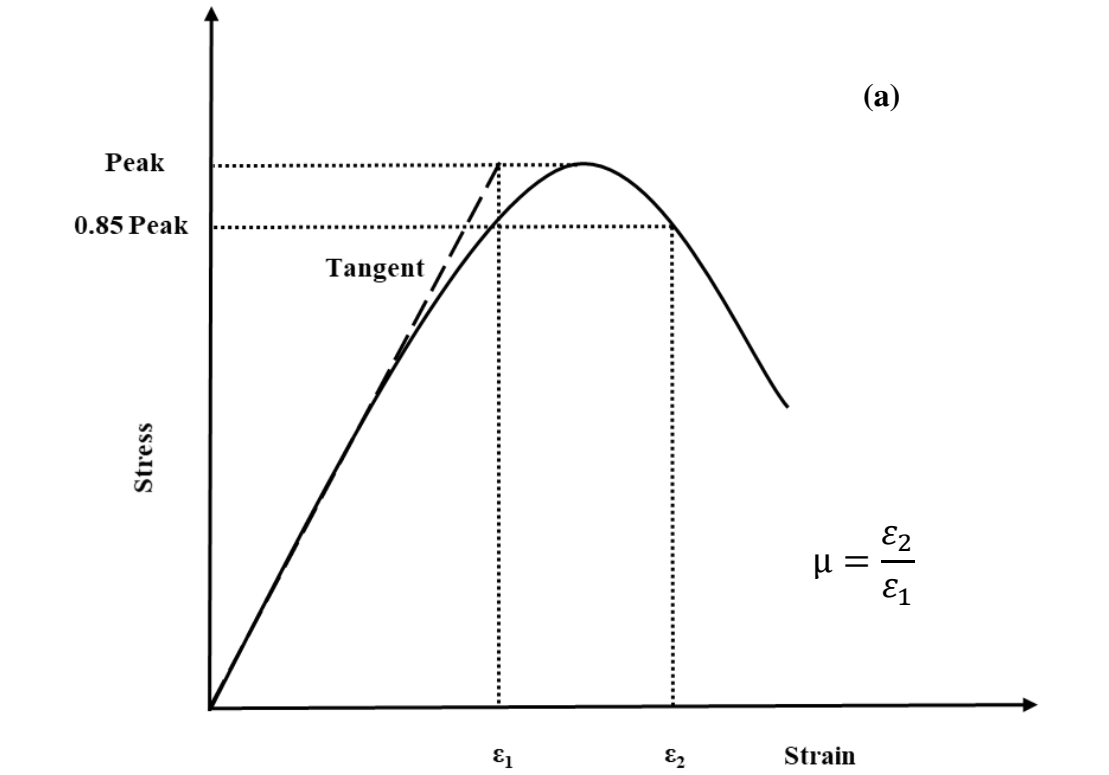

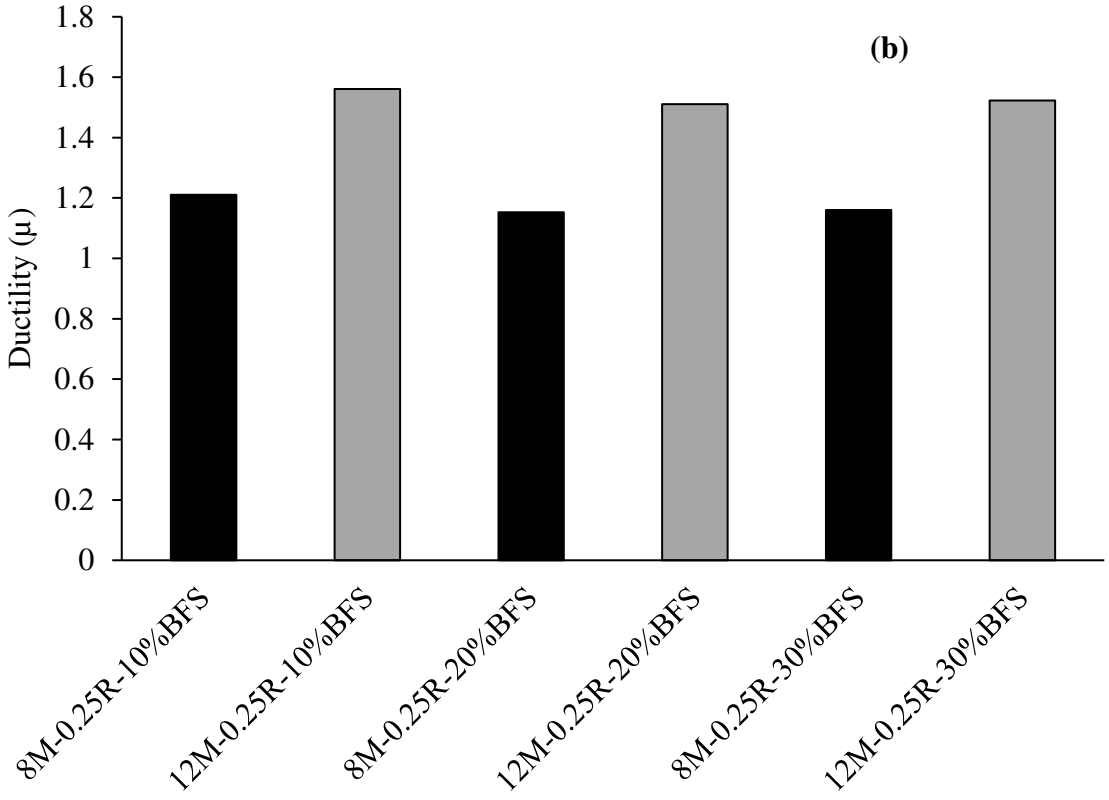

Fig. 7 Ductility of geopolymer samples (a) Measurement (b) Effect with change in molarity for varying slag content specimens

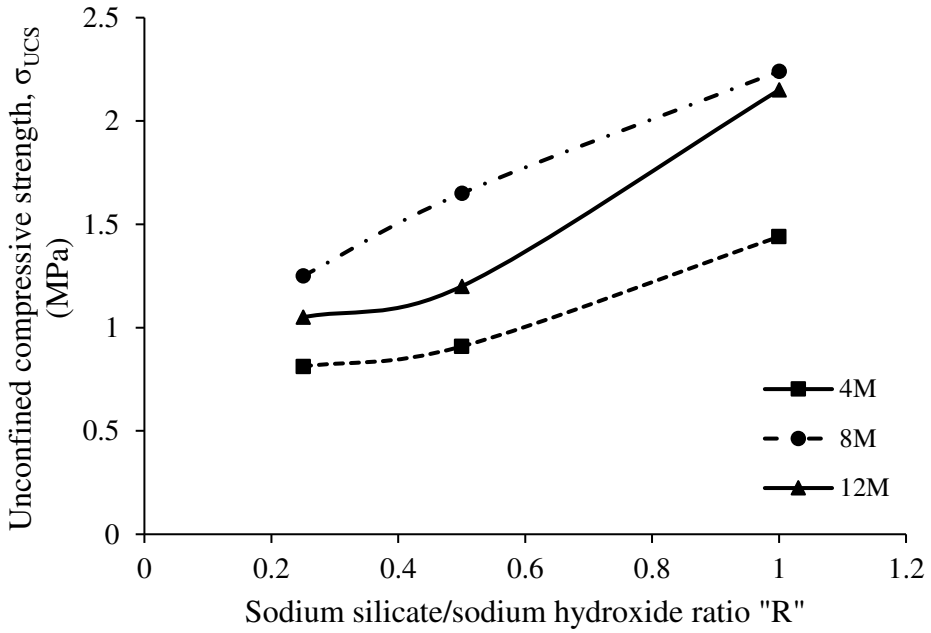

Figure 8 Compressive strength variation for basalt fines geopolymer w.r.t. Na_2SiO_3/NaOH ratios (R)

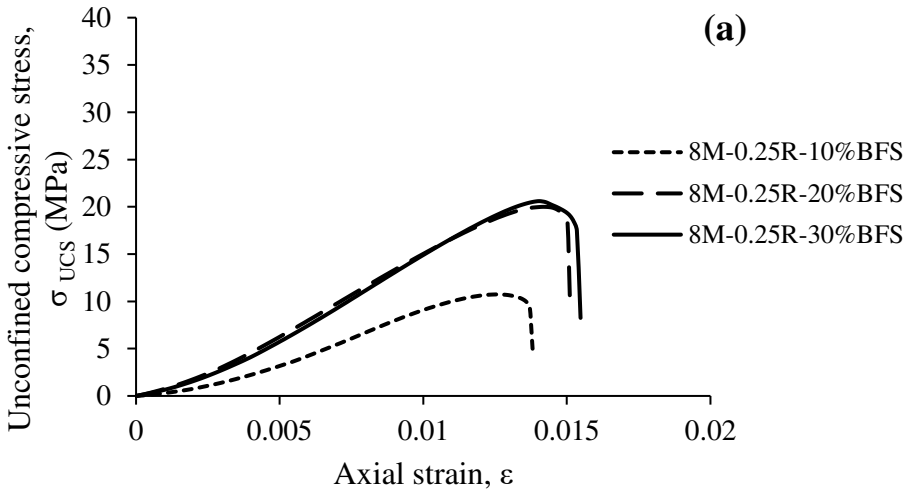

921

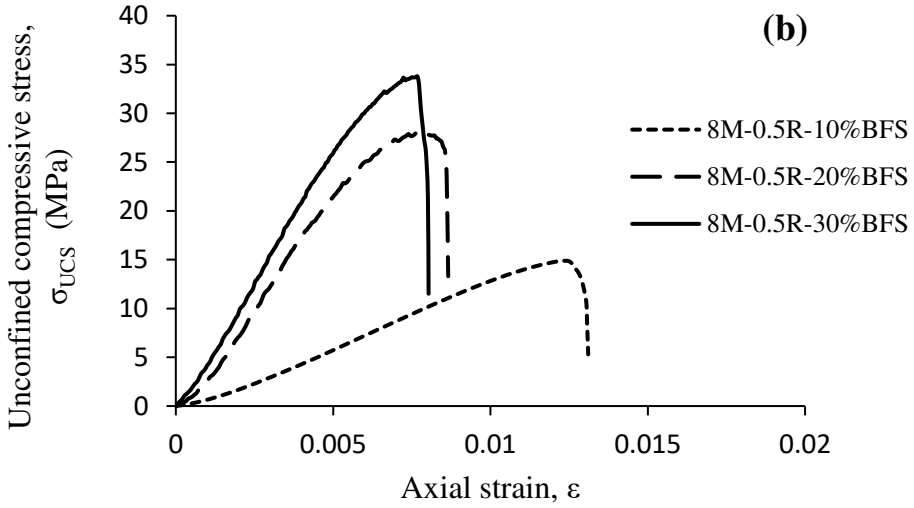

922

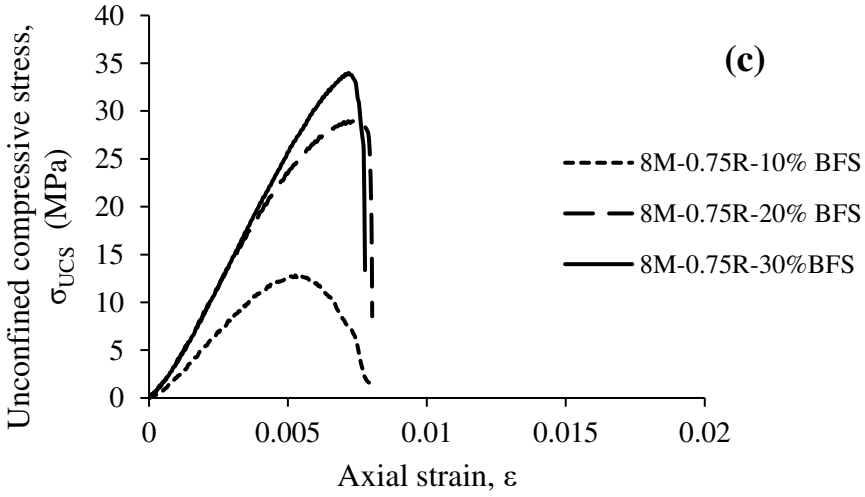

923

924 Figure 9 Stress-strain curves for basalt fines and different percentages of blast furnace slag
925 geopolymer with 8M NaOH concentration and Na_2SiO_3/NaOH ratio of (a) 0.25 (b) 0.5 and (c)
926 0.75

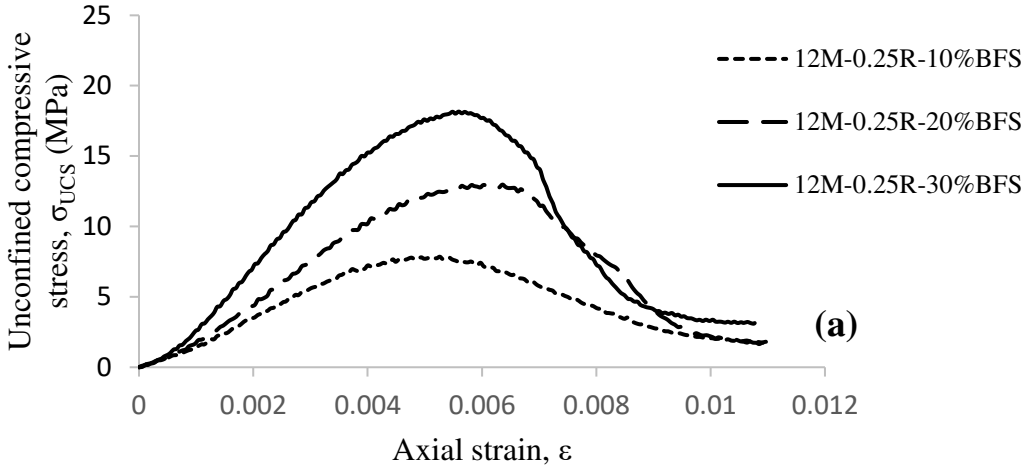

927

928

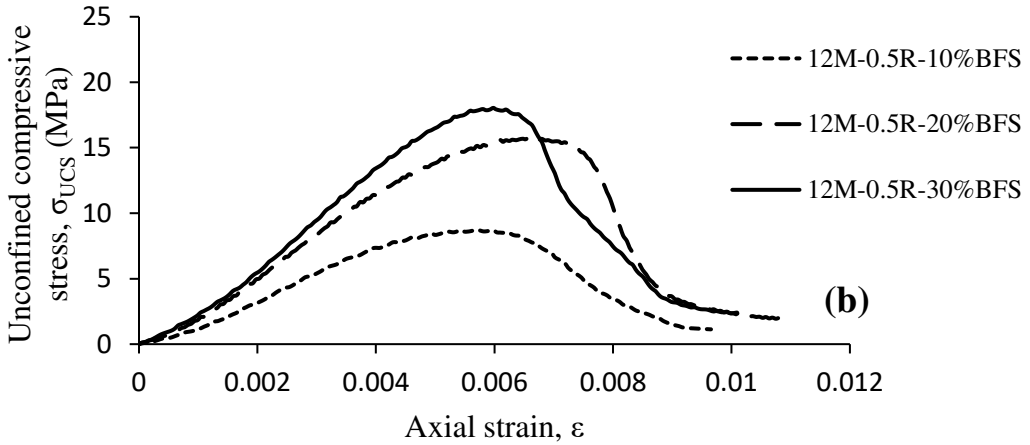

929

930

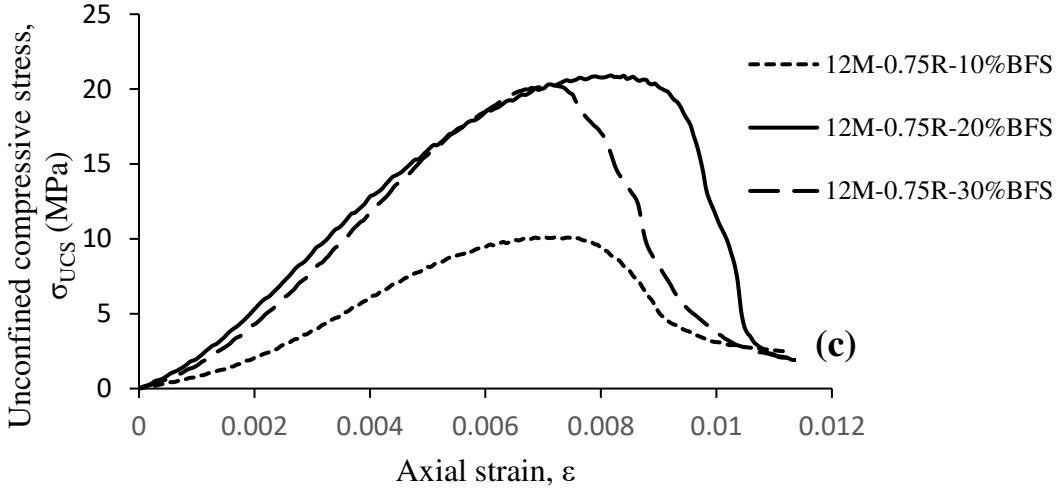

931

932 Figure 10 Stress-strain curves for basalt fines and different percentages of blast furnace slag
933 geopolymer with 12M NaOH concentration and Na_2SiO_3/NaOH ratio of (a) 0.25 (b) 0.5 and
934 (c) 0.75

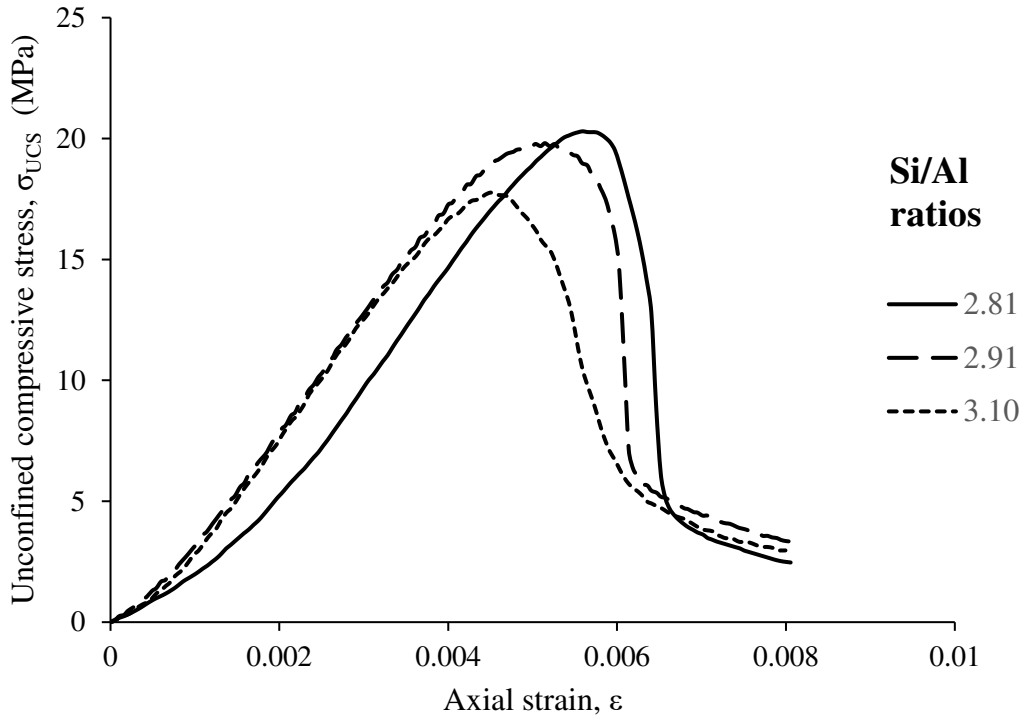

Figure 11 Stress-strain curves for basalt fines and blast furnace slag geopolymers with varying Si/Al ratios

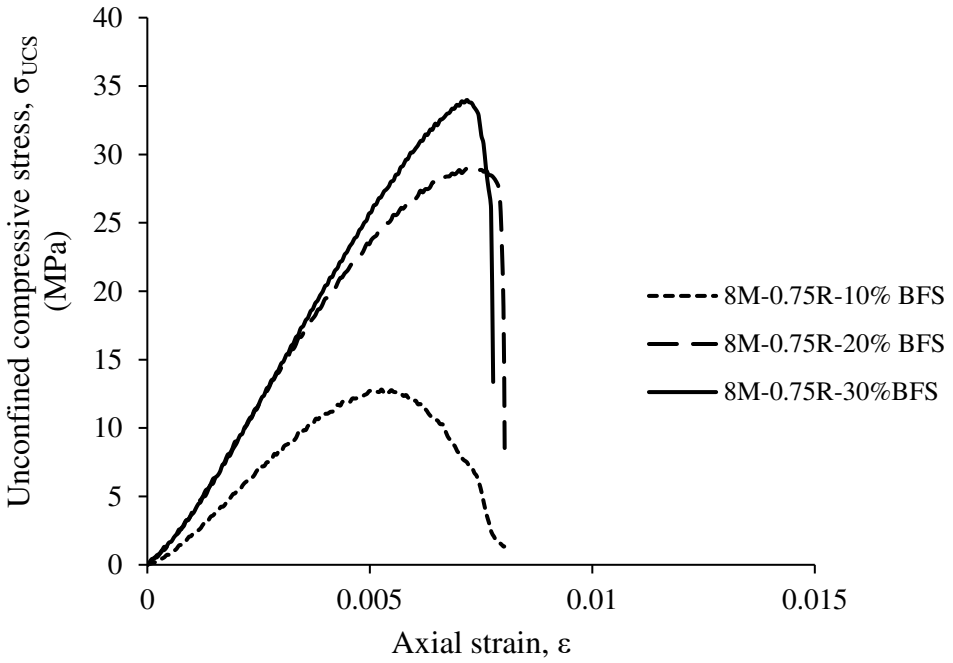

954

955 Figure 12 Stress-strain curves for basalt fines and different percentages of blast furnace slag
956 geopolymer with 8M NaOH concentration and Na_2SiO_3/NaOH ratio of 0.75

957

958

959

960

961

962

963

964

965

966

967

968

969

970

971

972

973

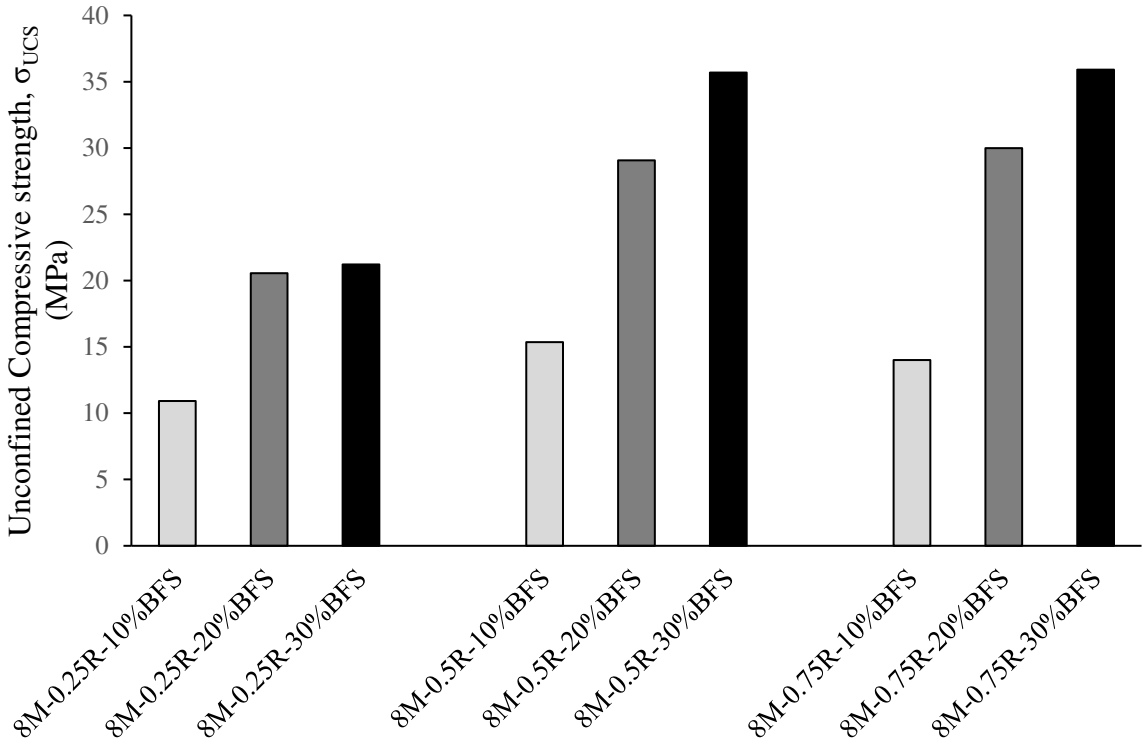

Figure 13 Comparison chart of compressive strength of basalt fines geopolymer with 8M NaOH concentration and various Na_2SiO_3/NaOH ratios at different percentages of blast furnace slag

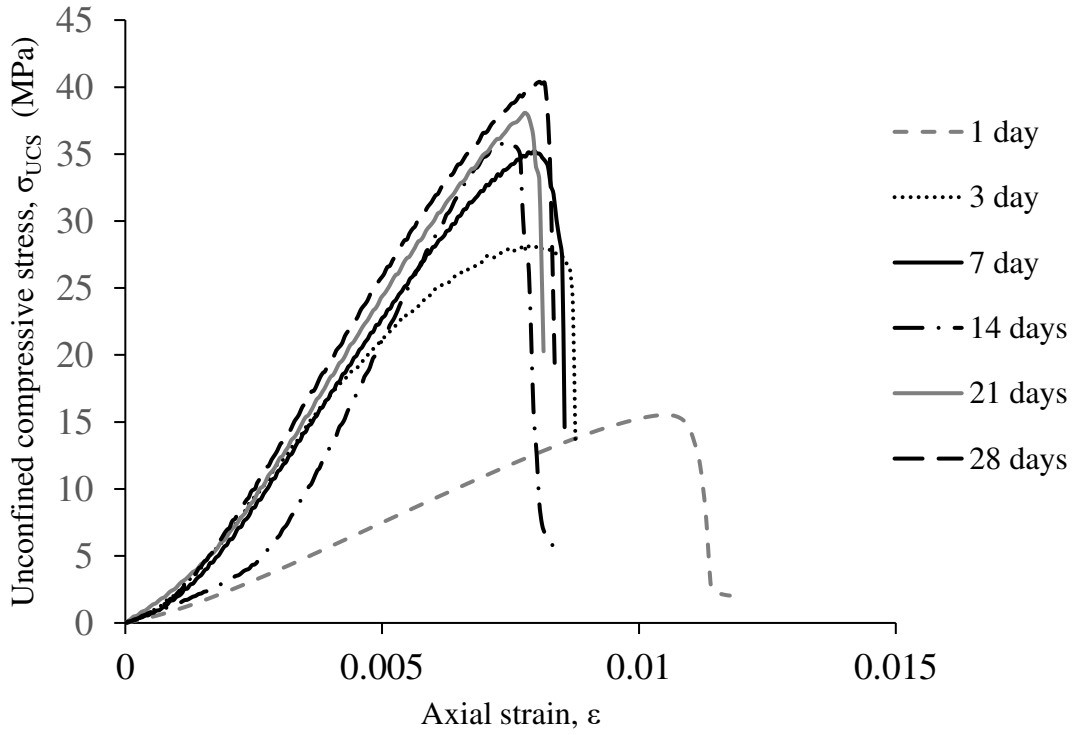

Figure 14 Stress-strain variation for basalt fines and 30% blast furnace slag geopolymer with respect to curing time

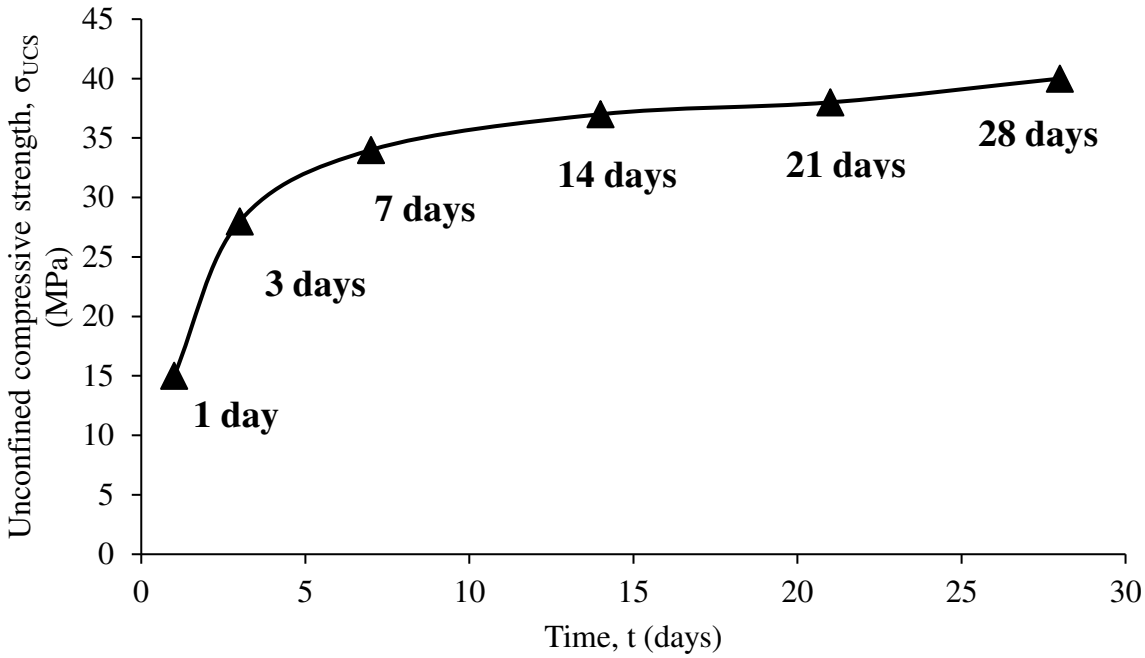

Figure 15 Variation in peak axial stress of basalt fines and 30% blast furnace slag geopolymer with time

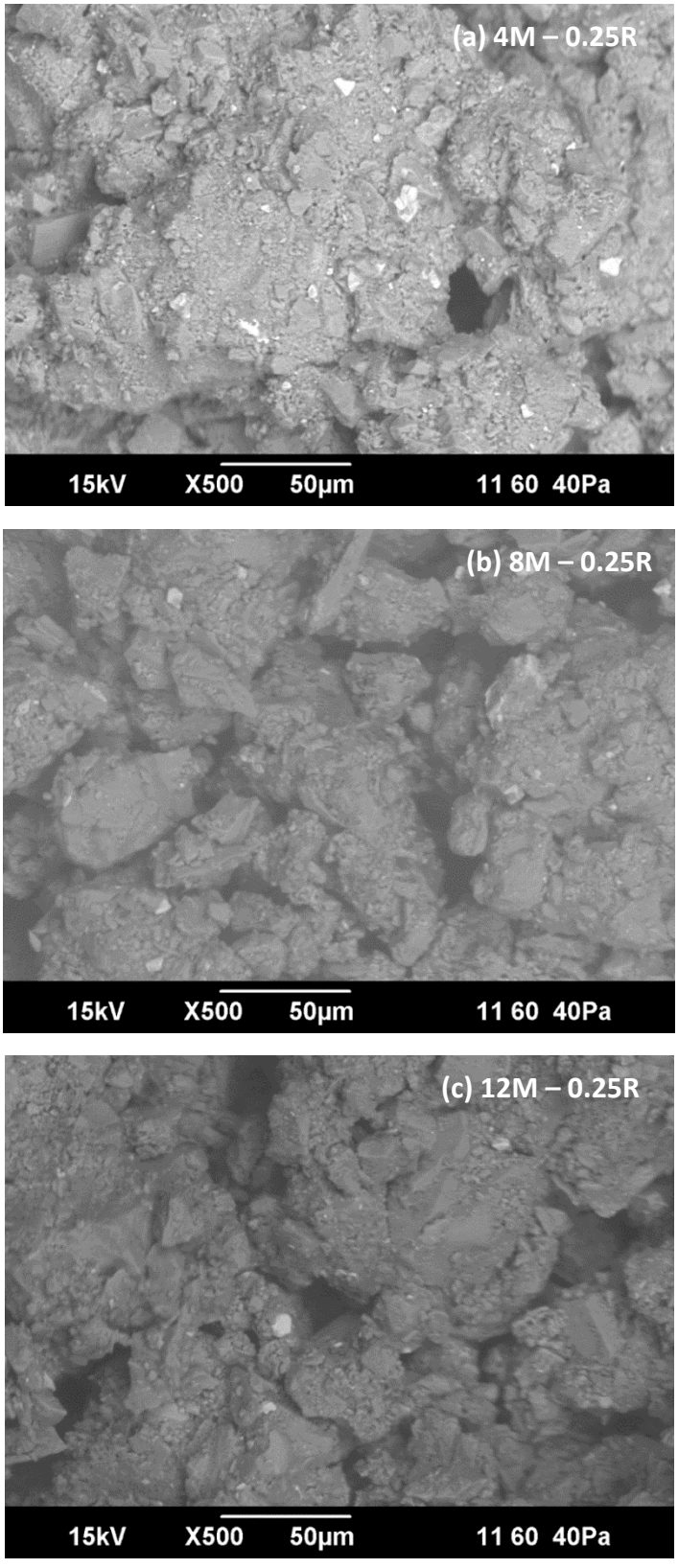

Figure 16 SEM images for basalt fines geopolymer at different molar concentrations of alkaline activator (a) 4M-0.25R (b) 8M-0.25R and (c) 12M-0.25R (Micrographs taken by Mohsin Nawaz)

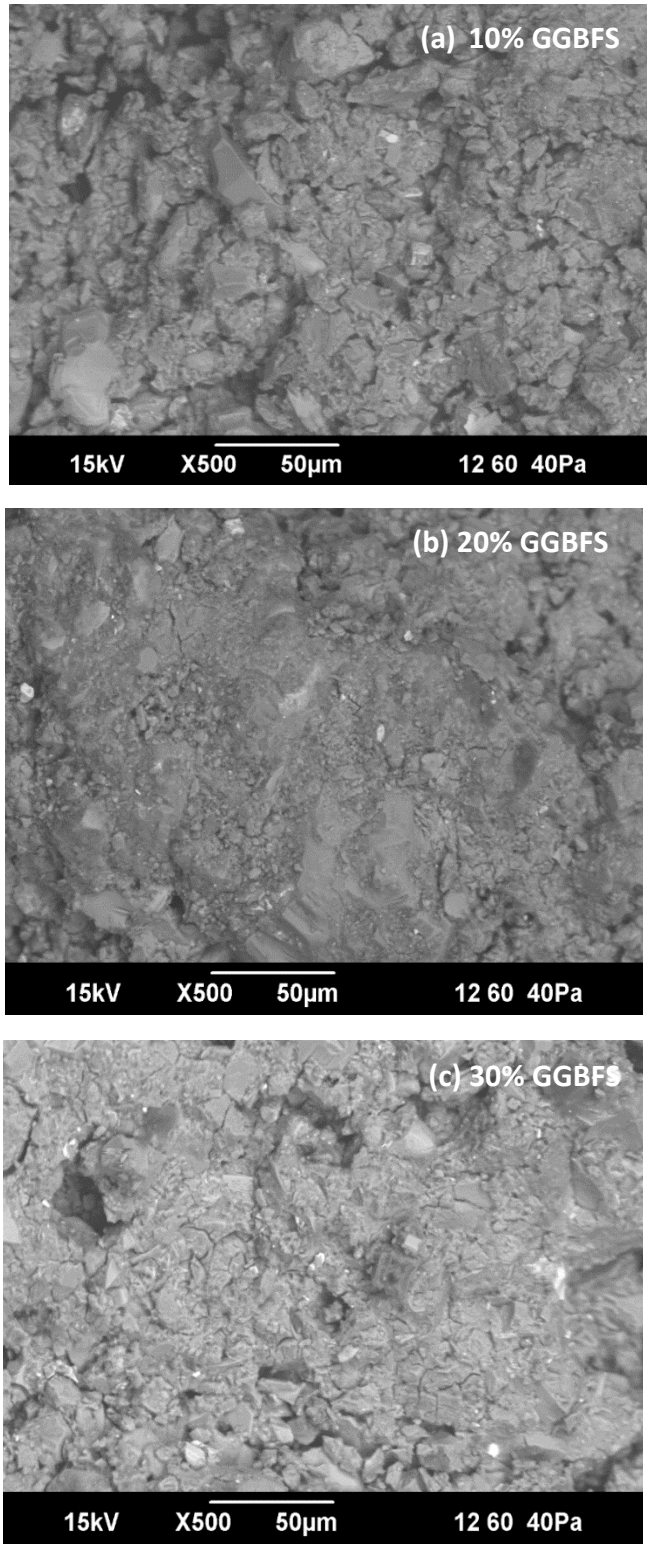

Figure 17 SEM images for basalt fines geopolymer (8M-0.75R) with different percentages of ground-granulated blast furnace slag (a) 10% (b) 20% and (c) 30% (Micrographs taken by Mohsin Nawaz)

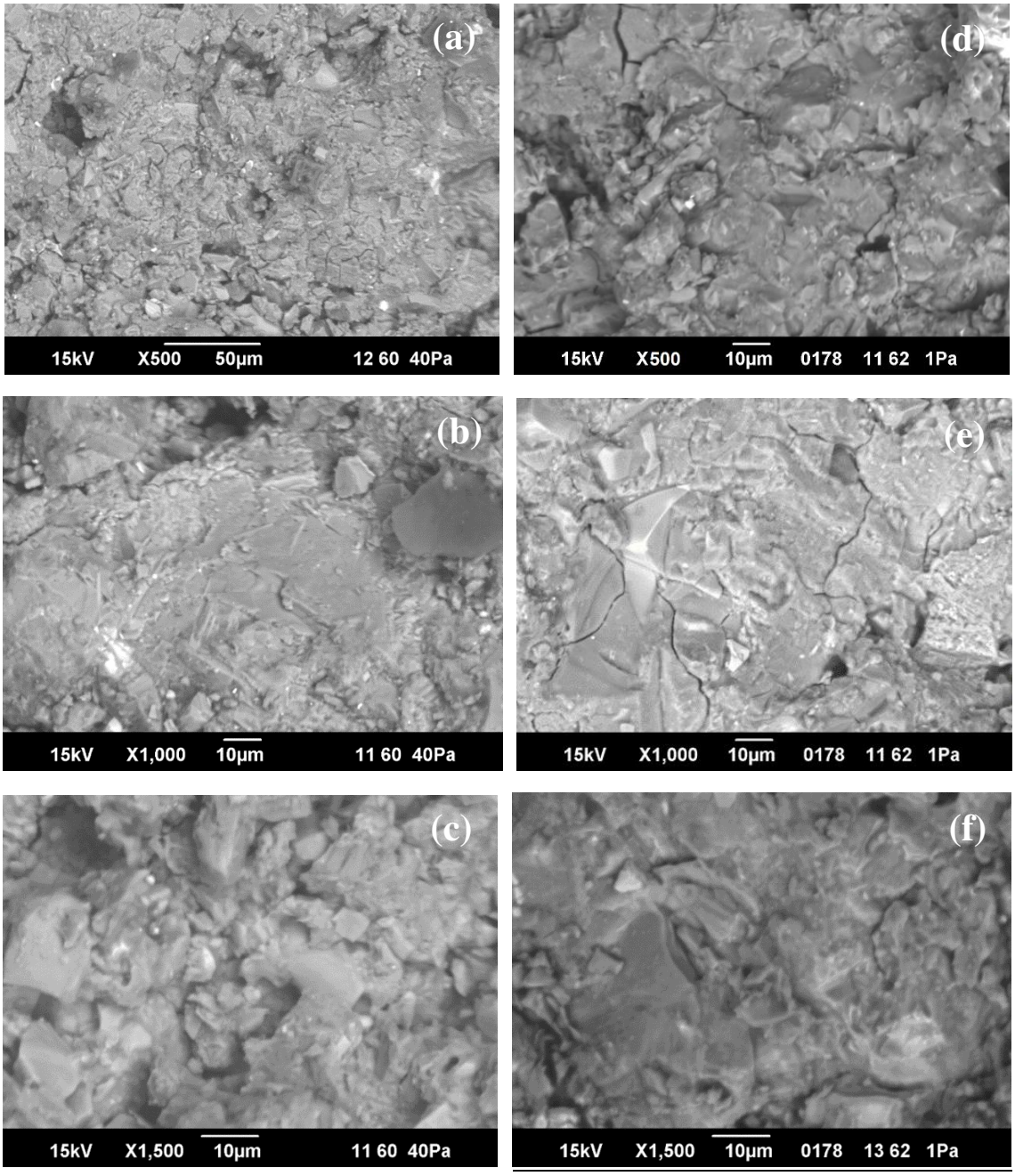

Figure 18 Microstructure of basalt fines and blast furnace slag geopolymer (8M-0.75R-30%BFS) after 7 days (a) x500 (b) x1000 (c) x1500 and 28 days (d) x500 (e) x1000 and (f) x1500 (Micrographs taken by Mohsin Nawaz)

List of Figures

Figure 17 SEM images for basalt fines geopolymer (8M-0.75R) with different percentages of ground granulated blast furnace slag (a) 10% (b) 20% and (c) 30% (Micrographs taken by Mohsin Nawaz)

Figure 18 Microstructure of basalt fines and blast furnace slag geopolymer (8M-0.75R-30%BFS) after 7 days (a) x500 (b) x1000 (c) x1500 and 28 days (d) x500 (e) x1000 and (f) x1500 (Micrographs taken by Mohsin Nawaz)